© 2020. Published by The Company of Biologists Ltd | Development (2020) 147, dev184242. doi:10.1242/dev.184242

RESEARCH ARTICLE

Core Hippo pathway components act as a brake on Yap and Taz in the development and maintenance of the biliary network

Zachary J. Brandt[1], Ashley E. Echert[1], Jonathan R. Bostrom[1], Paula N. North[2] and Brian A. Link[1,*]

ABSTRACT

The development of the biliary system is a complex yet poorly understood process, with relevance to multiple diseases, including biliary atresia, choledochal cysts and gallbladder agenesis. We present here a crucial role for Hippo-Yap/Taz signaling in this context. Analysis of *sav1* mutant zebrafish revealed dysplastic morphology and expansion of both intrahepatic and extrahepatic biliary cells, and ultimately larval lethality. Biliary dysgenesis, but not larval lethality, is driven primarily by Yap signaling. Re-expression of Sav1 protein in *sav1*$^{-/-}$ hepatocytes is able to overcome these initial deficits and allows *sav1*$^{-/-}$ fish to survive, suggesting cell non-autonomous signaling from hepatocytes. Examination of *sav1*$^{-/-}$ rescued adults reveals loss of gallbladder and formation of dysplastic cell masses expressing biliary markers, suggesting roles for Hippo signaling in extrahepatic biliary carcinomas. Deletion of *stk3* revealed that the phenotypes observed in *sav1* mutant fish function primarily through canonical Hippo signaling and supports a role for phosphatase PP2A, but also suggests Sav1 has functions in addition to facilitating Stk3 activity. Overall, this study defines a role for Hippo-Yap signaling in the maintenance of both intra- and extrahepatic biliary ducts.

KEY WORDS: Hippo pathway, Cholangiocarcinoma, Gallbladder, Hepatopancreatic ductal system, Sav1, Stk3

INTRODUCTION

Collectively the biliary system comprises the ductal network connecting the liver and gallbladder to the digestive tract. This system includes the extrahepatic ducts, intrahepatic ducts, as well as the cystic and common bile ducts. Together with hepatocytes, they form the hepatobiliary system and are responsible for the formation, secretion and storage of bile. A primary function of bile is fat emulsification via bile acids. However, bile also contains cholesterol, bilirubin, amino acids, vitamins and signaling molecules. Homeostasis of both the intra- and extrahepatic components of this system is crucial for proper bile transport. The network is continuous with the pancreatic ductal system, and collectively they are termed the hepatopancreatic ductal system (Keplinger and Bloomston, 2014). Zebrafish have been particularly useful for studying associated diseases, including progressive familiar intrahepatic cholestasis type 2, Alagille syndrome and biliary atresia (Cofer et al., 2016; Ellis et al., 2018; Lorent et al., 2004, 2015; Pham and Yin, 2019). While the signaling pathways and molecular mechanisms governing the development of the biliary system remain incompletely understood, they appear to be well conserved between species (Villasenor and Stainier, 2017).

Organogenesis of the biliary system is closely intertwined with formation of the liver and pancreas (Lemaigre, 2019; Villasenor and Stainier, 2017). As the biliary system can be divided into intrahepatic and extrahepatic parts, so can its development. The intrahepatic biliary epithelial cells are derived from bipotent liver progenitor cells termed hepatoblasts. The extrahepatic ductal cells are derived from distinct, but less characterized progenitors (Villasenor and Stainier, 2017). In zebrafish, signaling factors controlling intrahepatic biliary cell differentiation have been identified (Ko et al., 2019; Lorent et al., 2010; Manfroid et al., 2012; Russell et al., 2019). However, less is known regarding extrahepatic biliary system specification. Research in mice shows that the extrahepatic biliary system shares its origin with the ventral pancreas, rather than the liver (Spence et al., 2009). In zebrafish, presumptive hepatopancreatic ductal progenitor cells are first identified by position and expression of annexin A4 34 h post-fertilization (hpf), after specification of the liver bud (Zhang et al., 2014). Mutations of *fgf10*, *sox9b* and *hhex* in zebrafish reveal crucial roles for these genes in the development of the extrahepatic biliary system in fish, although some effects may be secondary to dysgenic pancreas or liver (Delous et al., 2012; Dong et al., 2007; Gao et al.; Manfroid et al., 2012; Shin et al., 2011; Villasenor et al., 2020). Recent work found Eph/ephrin B signaling regulates early morphogenesis of the tubular structures in the hepatopancreatic duct (Thestrup et al., 2019). Beyond these studies, little is known about the development and maintenance of the extrahepatic biliary system.

Analysis of *nf2* zebrafish mutants has revealed that they possess dilated common bile ducts, choledochal cysts and hepatomegaly (Sadler et al., 2005). The authors suggested that the tumor suppressor may control proliferation of a bipotent progenitor cell that could give rise to both hepatocytes and biliary cells; however, this does not explain the defects observed in the extrahepatic common bile duct. Nf2 has since been shown to act upstream of Hippo signaling (Hamaratoglu et al., 2006). Heterozygous *nf2* mutant mice develop hepatocellular carcinoma (McClatchey et al., 1998). Independent studies of *Albumin*-Cre-mediated deletion of *nf2* in mice revealed development of cholangiocarcinoma and expansion of biliary epithelial and presumptive progenitor cells (Benhamouche et al., 2010; Zhang et al., 2010). These studies, however, offered conflicting evidence on the involvement of the Hippo-Yap pathway. Given the incomplete understanding of hepatopancreatic ductal development and maintenance, and the potential but unclear role of the Hippo pathway, we sought to study these issues.

The canonical Hippo pathway is a phosphorylation cascade composed of kinases serine/threonine kinase 3 and 4 (Stk3 in zebrafish, Mst1/2 in mammals) and their scaffolding protein salvador family WW domain containing protein 1 (Sav1 in zebrafish, WW45 in mammals), which, through phosphorylation,

[1]Department of Cell Biology, Neurobiology and Anatomy, Medical College of Wisconsin, Wauwatosa, WI 53226, USA. [2]Department of Pediatric Pathology, Medical College of Wisconsin, Wauwatosa, WI 53226, USA.

*Author for correspondence (blink@mcw.edu)

B.A.L., 0000-0002-7173-2642

Handling Editor: Steve Wilson
Received 24 August 2019; Accepted 24 April 2020

Development (2020) 147, dev184242. doi:10.1242/dev.184242

regulates the activity of large tumor suppressor kinases 1 and 2 (Lats1/2). Lats1/2 with MOB kinase activators 1 and 2 (Mob1a/b) phosphorylate the transcriptional co-activators Yes-associated protein 1 (Yap) and its paralog, WW domain containing transcription regulator 1 (WWTR1; more commonly known as Taz). This phosphorylation leads to cytoplasmic sequestration of and/or degradation of Yap and Taz. Non-phosphorylated Yap and Taz translocate to the nucleus and, as they cannot bind DNA directly, associate with several families of transcription factors to both activate and repress expression of various genes.

While Hippo signaling has not been studied in depth in extrahepatic biliary development, its role in liver development is better characterized. Transgenic overexpression of Yap in mice led to tissue overgrowth, including hepatomegaly and eventually hepatocellular carcinoma (Camargo et al., 2007). However, global mutants of Hippo pathway genes in mice exhibit embryonic or perinatal lethality, making later developmental studies difficult (Lee et al., 2008; McPherson et al., 2004; Oh et al., 2009). Since this discovery, the conditional deletions of the canonical Hippo kinases and their effectors in the mouse liver have been shown by multiple groups to cause hepatomegaly and both hepatocellular and cholangiocarcinoma, primarily through regulation of Yap (Benhamouche et al., 2010; Lee et al., 2010; Nishio et al., 2016; Wu et al., 2017; Yi et al., 2016). In this context, the role of the Hippo pathway in the development of the biliary system is restricted by available Cre lines. The commonly used *Albumin*-Cre line has limited activity in hepatoblasts and strong activity in hepatocytes, but nonetheless has been successfully used along with Adeno-Cre studies to demonstrate a role for the Hippo pathway in liver development. These studies showed through either Yap overexpression or Hippo pathway inhibition, that Yap activity expands immature biliary epithelial cells and leads to dedifferentiation of hepatocytes to a more progenitor-like state, suggesting Hippo-Yap/Taz signaling plays a key role in intrahepatic biliary duct development (Camargo et al., 2007; Lee et al., 2016; Wu et al., 2017; Yimlamai et al., 2014). Consistent with these findings, liver-specific deletion of Yap resulted in loss of mature biliary ducts and abnormal immature ductal structures, along with progressive peri-portal fibrosis, showing that Yap is required for bile duct development in mice (Zhang et al., 2010). These results reveal a crucial role for Hippo-Yap/Taz signaling in intrahepatic biliary duct development; however, the effects of Hippo signaling on the development and maintenance of the extrahepatic biliary system remain unknown.

To study a potential role for Hippo-Yap/Taz signaling in extrahepatic biliary and gallbladder development, we generated *sav1* and *stk3* zebrafish mutants. We find compelling evidence for the importance of Hippo signaling within multiple cell types of the hepatopancreatic ductal system. These findings have relevance to human diseases of this system, such as choledochal cysts, intra- and extrahepatic cholangiocarcinoma, as well as the molecular mechanisms of Hippo signaling.

RESULTS

Global deletion of zebrafish *sav1* causes larval lethality and abnormal gallbladder development

To investigate the role of Sav1 in zebrafish development, we generated a loss-of-function mutant and analyzed gross morphological changes throughout embryonic and larval development. Utilizing clustered regularly interspaced short palindromic repeats (CRISPR)/Cas9 gene editing, we targeted exon2 of *sav1*. A nonsense frameshift mutant allele caused by an 11bp insertion in *sav1* was identified and bred to establish a mutant line (Fig. 1A). Fish heterozygous for this allele were in-crossed to generate homozygous mutants referred to as *sav1*$^{-/-}$. When progeny from heterozygous matings were allowed to mature to adulthood, no *sav1*$^{-/-}$ mutants were recovered at 60 days post-fertilization (dpf). Analysis revealed a loss of Mendelian ratios from 14 dpf with no *sav1*$^{-/-}$ embryos surviving past 21 dpf. Observation of these fish revealed a dramatic reduction in the gallbladder of *sav1*$^{-/-}$ embryos compared with wild-type siblings at 7 dpf, with some embryos completely lacking a recognizable gallbladder (Fig. 1B,C). To better identify the gallbladder, we bathed embryos in fluorescent fatty acid BODIPY FL C5-ceramide. Upon uptake into the blood, BODIPY FL C5 is secreted by hepatocytes into the intrahepatic biliary ducts and accumulates throughout the biliary system, including in the gallbladder. Labeling of the gallbladder with this technique reinforced the loss of gallbladder, as the majority of embryos lacked gallbladder labeling or had diminished fluorescence (Fig. 1D). Although the gallbladder phenotype at 7 dpf was the only overt difference between *sav1*$^{-/-}$ embryos and their wild-type siblings, it alone seems unlikely to cause the early lethality we observed. To better assess changes across all tissues, we collected serial histological sections from embryos at 7, 10 and 16 dpf. Histology revealed abnormal gallbladder morphology as well as abnormal morphology in both extrahepatic and intrahepatic biliary ducts at all time points, with apparent increases in severity with age. Although all tissues were assessed, changes to the hepatobiliary system were the only defects noted. Hematoxylin and Eosin stained sections of the hepatobiliary system at 8 dpf corroborated these findings. Subsequent immunofluorescent staining with the gallbladder and biliary cell marker AnnexinA4 confirmed the abnormal cells were biliary epithelial cells and indicated their expansion within the liver (Fig. 1E,F).

Altered biliary morphology and proliferation in *sav1* mutants

To further assess duct morphology, we used immunofluorescent staining of annexin A4 to label gallbladder and intrahepatic biliary ducts. We performed annexin A4 immunostaining at multiple time-points from 80 hpf to 8 dpf in order to define the phenotype onset and progression (Fig. 2). Importantly, initiation of gallbladder development appeared unaffected, as 80 hpf larvae appear identical to their wild-type siblings (Fig. 2A,A′). At 5 dpf, the earliest abnormal phenotype presents with thickened intrahepatic biliary morphology and punctate staining at the normal position of the extrahepatic duct (Fig. 2B″). Some larvae also show loss of annexin A4 signal from the gallbladder (Fig. 2B‴). Analysis of annexin A4 expression in 5 dpf *sav1*$^{-/-}$ biliary systems revealed a phenotypic spectrum. The full spectrum is most prominent at 8 dpf. We categorized phenotypes as mild, moderate and severely dysgenic. Mild mutants had identifiable gallbladders, but decreased AnnexinA4 immunoreactivity, as well as altered intrahepatic biliary cell morphology, most notably increased duct diameter (Fig. 2E″). Moderate mutants lacked an annexin A4^{+} gallbladder but had elevated annexin A4 staining surrounding the presumptive gallbladder location (Fig. 2E‴). Moderate mutants also have abnormal intrahepatic ductal morphology, similar to mild mutants. Finally, the most severe mutants show loss of intra- and extrahepatic ductal structure (Fig. 2E⁗). We note too that some mutants appear phenotypically normal by this analysis (Fig. 2E′), which we suspect is due to delayed onset of the phenotype. Ratios of the described phenotypes at each time point are denoted in Fig. 2. The ratios of the phenotypic spectrum increase in severity with age, suggesting that the spectrum characterized at 8 dpf represents multiple stages of phenotype progression (Fig. 2F). For this reason, we focused on 8 dpf for the majority of analyses. We propose this phenotypic spectrum, which is marked by loss of biliary epithelial

Development (2020) 147, dev184242. doi:10.1242/dev.184242

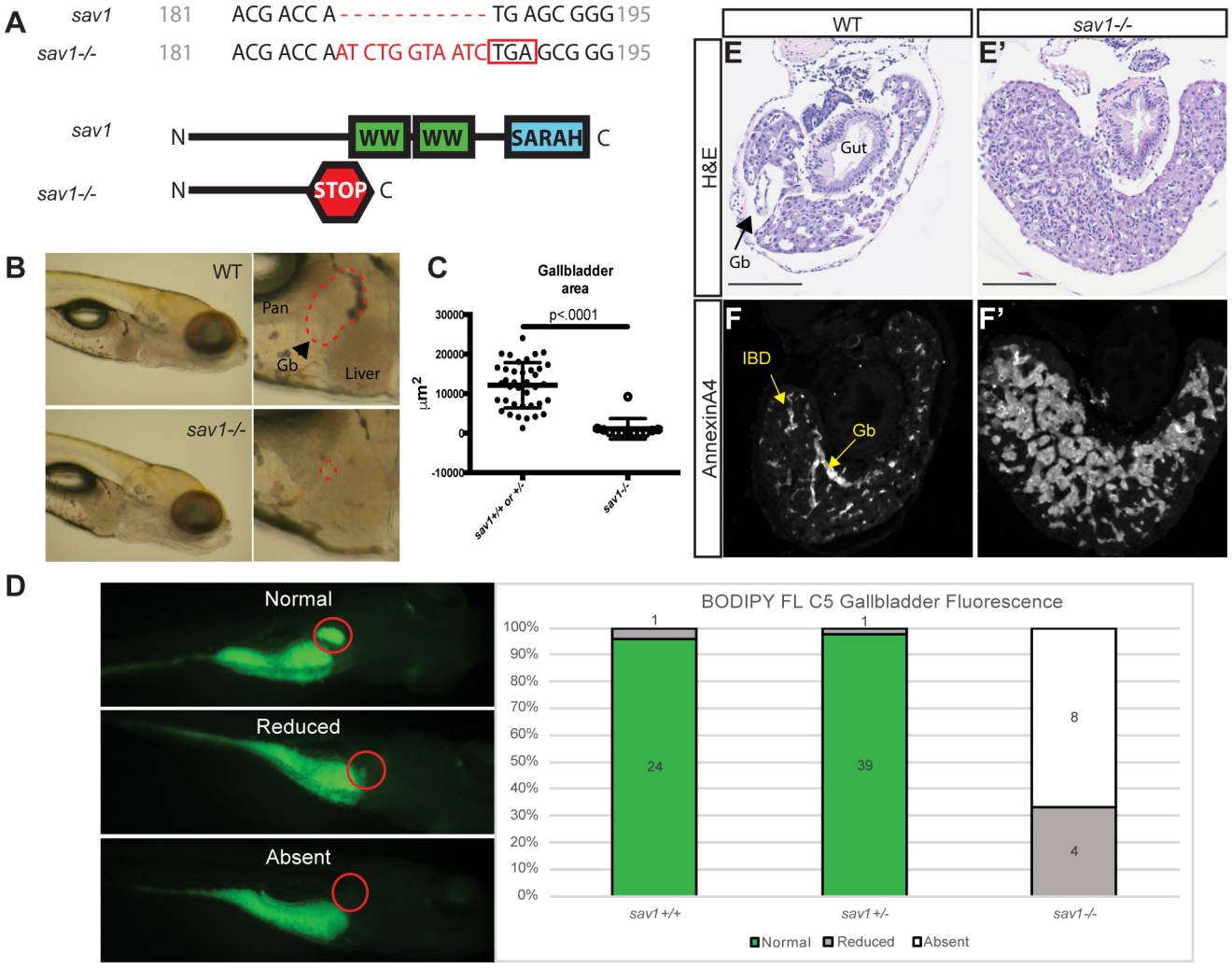

Fig. 1. Deletion of *sav1* causes larval lethality and abnormal gallbladder development. (A) Wild-type and mutant alleles of zebrafish *sav1*. *sav1* mutants contain an 11 bp insertion (red), causing a frameshift and early stop codon (red box). (B) Morphology of embryos at 8 dpf. Dashed red lines on higher magnification images outline the gallbladder. Pan, pancreas; Gb, gallbladder. (C) Quantification of gallbladder area shown in B; gallbladder location is indicated by red circles. Unpaired *t*-test with equal s.d., $P<0.0001$. $n=38$, $sav1^{+/+}$ or $^{+/-}$; $n=12$, $sav1^{-/-}$. Data are mean±s.d. (D) BODIPY FL C5 gallbladder uptake and ratiometric analysis at 8 dpf. Sample number (n) indicated within the graph. (E,E′) Hematoxylin and Eosin stained paraffin sections of normal gallbladder and liver in wild-type and $sav1^{-/-}$ mutants. Gb, gallbladder. Scale bars: 100 µm. (F,F′) Adjacent sections stained for annexin A4 confirm abnormal biliary morphology. Gb, gallbladder; IBD, intrahepatic bile duct. $n=5$ for both wild-type and $sav1^{-/-}$ paraffin histology.

cell marker annexin A4, but retention of activated leukocyte cell adhesion molecule (Alcam), is a progressive dysplasia resulting in the loss of proper identity of extra- and intrahepatic ducts, as well as gallbladder. These morphological changes are identifiable by transmission electron microscopy (TEM), and present as clusters of more electron dense biliary cells (Fig. 3E,E′).

Loss of annexin A4 defects could be due to apoptosis. When annexin A4 was identified as the antigen for the 2F11 antibody, it was reported that annexin A4 was required for liver progenitor viability through inhibition of the extrinsic apoptotic pathway (Zhang et al., 2014). However, we did not find differences in TUNEL staining between $sav1^{-/-}$ fish and wild-type siblings at 5 or 8 dpf (Fig. S1). Importantly, there were no changes in TUNEL staining across the phenotypic spectrum, indicating that loss of annexin A4 staining is not indicative of cell death in $sav1^{-/-}$ mutants.

To examine proliferation in the $sav1^{-/-}$ biliary system, we assessed changes in DNA synthesis by EdU incorporation. $sav1^{-/-}$ fish across the phenotypic spectrum displayed increased EdU incorporation throughout the entire liver when compared with wild-type siblings, consistent with their larger liver size. Particularly high levels of EdU were noted surrounding the mutant gallbladder (Fig. 3B-B′′′′) and within the gallbladder (Fig. 3D). However, increased proliferation is not specific to the gallbladder or biliary ducts, but rather occurs throughout the liver, suggesting $sav1^{-/-}$ hepatocytes also have elevated proliferation.

Previous reports on Hippo signaling in biliary development suggested that immature and more proliferative biliary epithelial cells may explain the abnormal morphology in the gallbladder, and both the intra- and extrahepatic biliary systems of $sav1^{-/-}$ larvae (Camargo et al., 2007; Lee et al., 2016; Wu et al., 2017; Yimlamai et al., 2014). We therefore hypothesized that the $sav1^{-/-}$ biliary phenotype may be explained by a progressive de-differentiation of biliary epithelial cells. We reasoned that, as the intrahepatic biliary cells are derived from bipotent hepatoblasts, an increase in the hepatoblast marker Prox1 in abnormal $sav1^{-/-}$ biliary cells might be observed. However, we found that Prox1 staining remains in

Development (2020) 147, dev184242. doi:10.1242/dev.184242

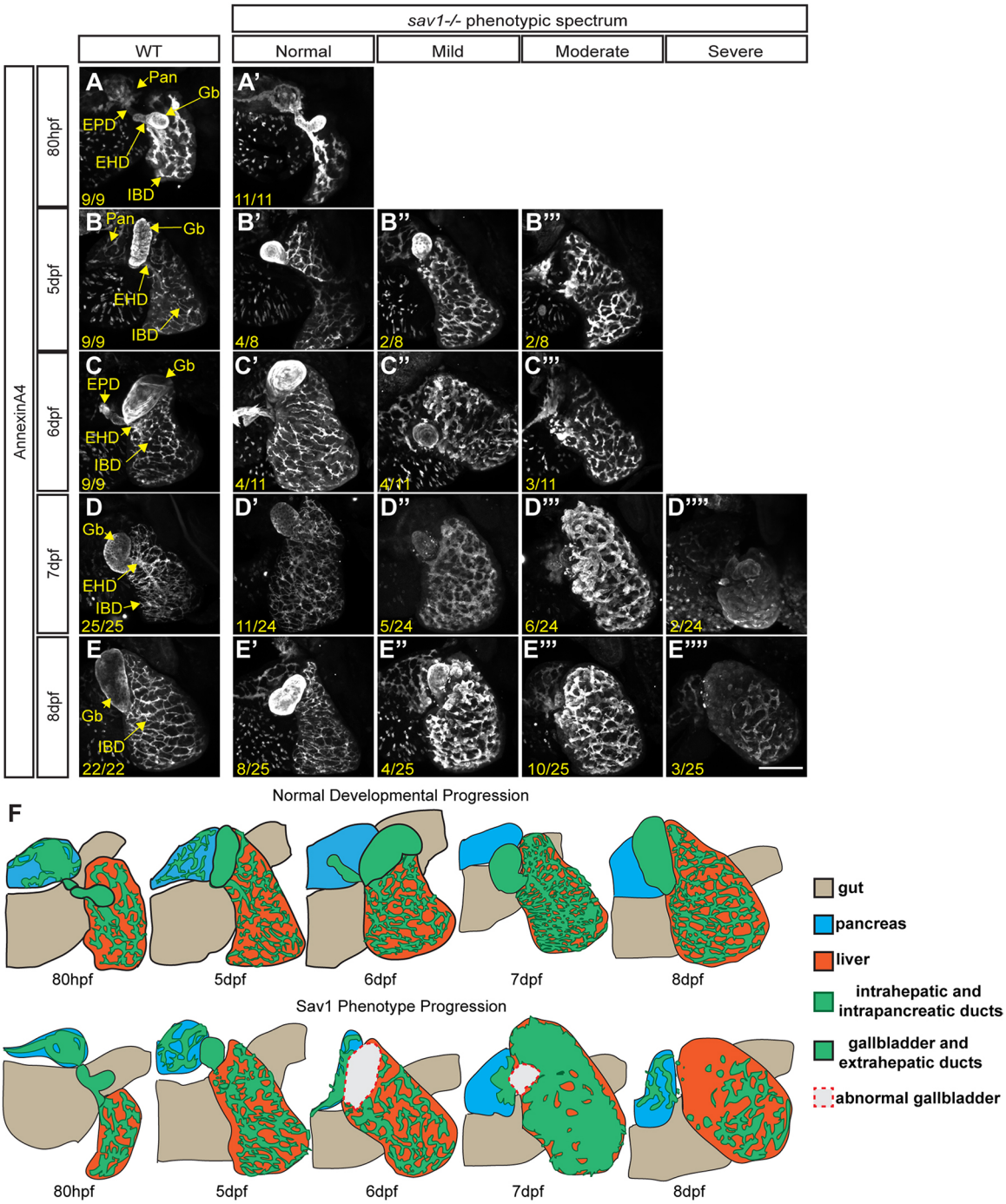

Fig. 2. *sav1* mutants display a wide spectrum of biliary morphology representative of phenotype progression. (A-E‴) Whole-mount annexin A4 staining of liver and gallbladder from 80 hpf to 8 dpf. Pan, pancreas; Gb, gallbladder; EHD, extrahepatic duct; EPD, extrapancreatic duct; IBD, intrahepatic bile duct. Numbers indicate the ratio of fish that displayed the phenotype/total fish analyzed. (F) Cartoon depictions of each time-point.

both hepatocytes and intrahepatic biliary cells of wild-type and *sav1*$^{-/-}$ larvae (Fig. S2). In fact, *sav1*$^{-/-}$ specimens displayed a slight loss of Prox1 staining in the more severe mutants. This suggests that although the abnormal morphology and loss of annexin A4 imply disruption of proper biliary identity, this is not due to a simple de-differentiation of the intrahepatic biliary cells. The changes in gallbladder and biliary cell morphology, marker protein expression and proliferation suggest that *sav1*$^{-/-}$ gallbladder and biliary cells lose proper biliary identity and become dysplastic and proliferative.

Yap but not Taz drives *sav1*$^{-/-}$ phenotypes

Sav1 functions primarily as an adaptor protein in the Hippo signaling pathway, which regulates kinase activity and thus subcellular localization and levels of the main pathway effectors Yap and Taz. Therefore, we sought to examine Yap and Taz activity in *sav1*$^{-/-}$ fish. We used the *ctgfa:d2GFP* transgenic line as a reporter for Yap and Taz activity. The *ctgfa* gene is an established target of Yap and Taz transcriptional activation, and we have previously shown this reporter exhibits increased fluorescence in response to Yap overexpression (Miesfeld et al., 2015). Wild-type

Development (2020) 147, dev184242. doi:10.1242/dev.184242

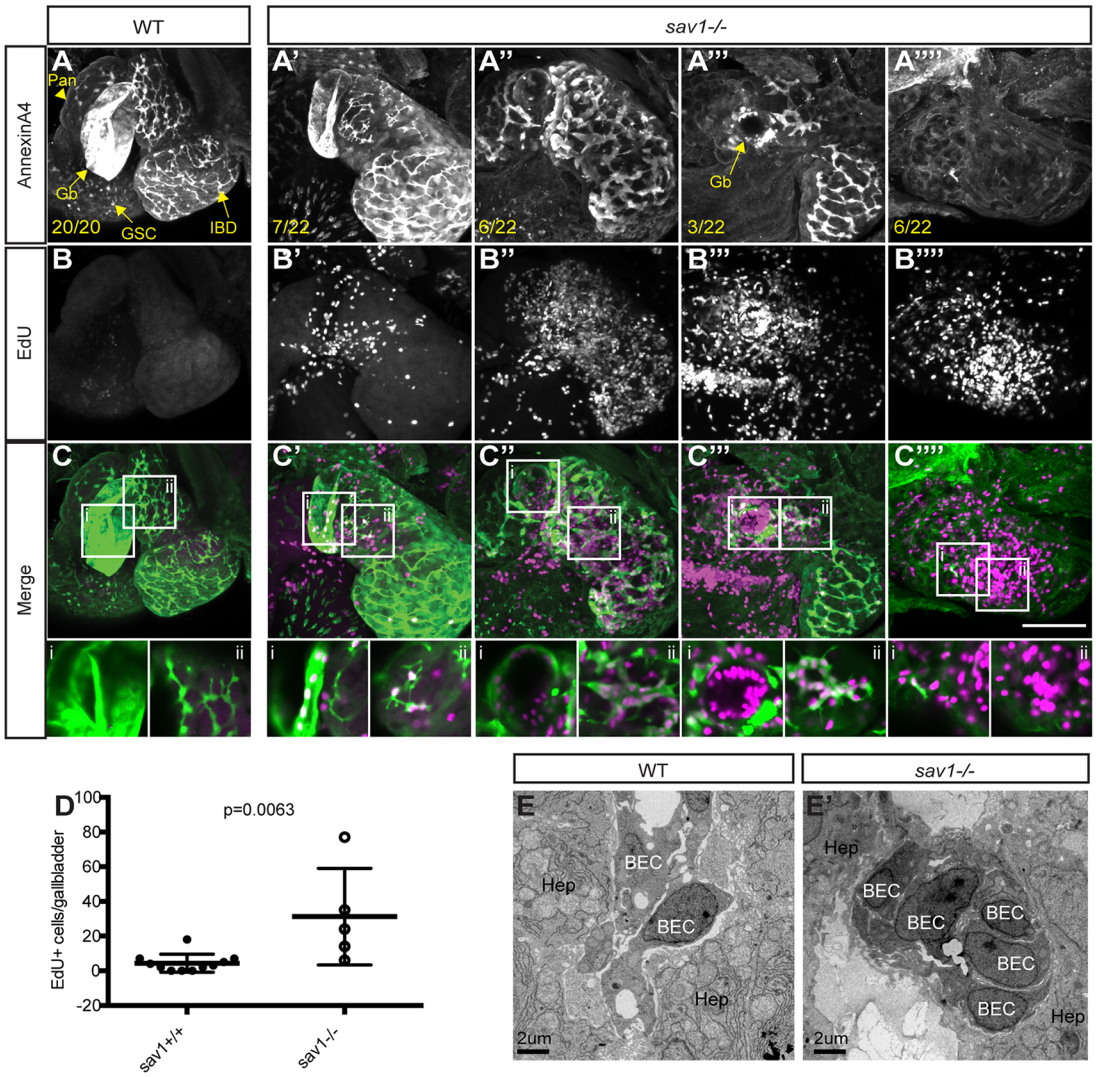

Fig. 3. The *sav1* mutant biliary system exhibits excess proliferation. (A-A‴) Whole-mount annexin A4 staining of liver and gallbladder at 8 dpf. Pan, pancreas; Gb, gallbladder; GSC, gut secretory cell; IBD, intrahepatic bile duct. *n* is indicated and displayed as the ratio of fish containing the displayed phenotype/total fish analyzed. (B-B‴) EdU staining of the specimen analyzed in A. (C-C‴) Merged images of A and B with annexin A4 staining in green and EdU stain in magenta. Scale bar: 100 µm. Single plane enlarged images are found below each merged image, with the left image focused on a region of gallbladder and the right image focused on intrahepatic biliary ducts. (D) Quantitation of EdU^{+} cells in annexin A4-labeled gallbladders; *n*=11 wild-type, *n*=5 *sav1*$^{-/-}$. Data are mean±s.d. Unpaired *t*-test with equal s.d. resulted in *P*=0.0063. (E,E′) TEM of wild-type (E) and *sav1*$^{-/-}$ (E′) livers at 10 dpf: *n*=3 wild type; *n*=3 *sav1*$^{-/-}$. BEC, biliary epithelial cell; Hep, hepatocyte.

larvae at 8 dpf show robust expression throughout the gallbladder as well as in sporadic cells throughout the liver (Fig. 4A). These sporadic cells morphologically resemble hepatic stellate cells and lack biliary epithelial cell markers (Fig. S3). Changes in *ctgfa:*d2GFP expression in *sav1*$^{-/-}$ mutant fish again displayed a spectrum of phenotypic changes with increased numbers of *ctgfa:*d2GFP^{+} cells throughout the liver (Fig. 4A′) and gradual increases in reporter expression in the gallbladder and immediate connecting ducts (Fig. 4A″) followed by loss of normal morphology and increased area of abnormal *ctgfa:*d2GFP^{+} cells (Fig. 4A‴). There were also increased numbers of *ctgfa:*d2GFP^{+}; annexin A4^{-} cells resembling hepatic stellate cells, suggesting that loss of *sav1* may also result in recruitment and/or activation of stellate cells (Fig. S3). Live imaging and fluorescent intensity analysis of *ctgfa:*d2GFP expression across mutant livers confirmed a significant increase in reporter activity compared with wild-type siblings, likely due to both increased cell number and fluorescent intensity of d2GFP^{+} cells (Fig. 4B,B′,C). We were unable to analyze changes in gallbladder fluorescence due to loss of identifiable gallbladder structure in many *sav1*$^{-/-}$ larvae. These results show that Yap and Taz transcriptional activity is increased in the abnormal biliary cells of *sav1*$^{-/-}$ fish, suggesting this activity may drive these phenotypes.

As Hippo signaling regulates Yap and Taz protein level and localization, we assessed these factors by immunostaining. We used two antibodies: one predicted to recognize both Yap and Taz (ab81183, Abcam), referred to as Yap and Taz staining; and another that specifically labels Taz in zebrafish (D24E4, Cell Signaling) (Kimelman et al., 2017; Lai et al., 2018; Miesfeld et al., 2015). We confirmed the specificity of Taz staining in the biliary system, as signal was lost in *taz*$^{-/-}$ but not *yap*$^{-/-}$ larvae (Fig. S4A-C). Interestingly, the staining pattern of these antibodies strikingly differs in the internal organ system of wild-

Development (2020) 147, dev184242. doi:10.1242/dev.184242

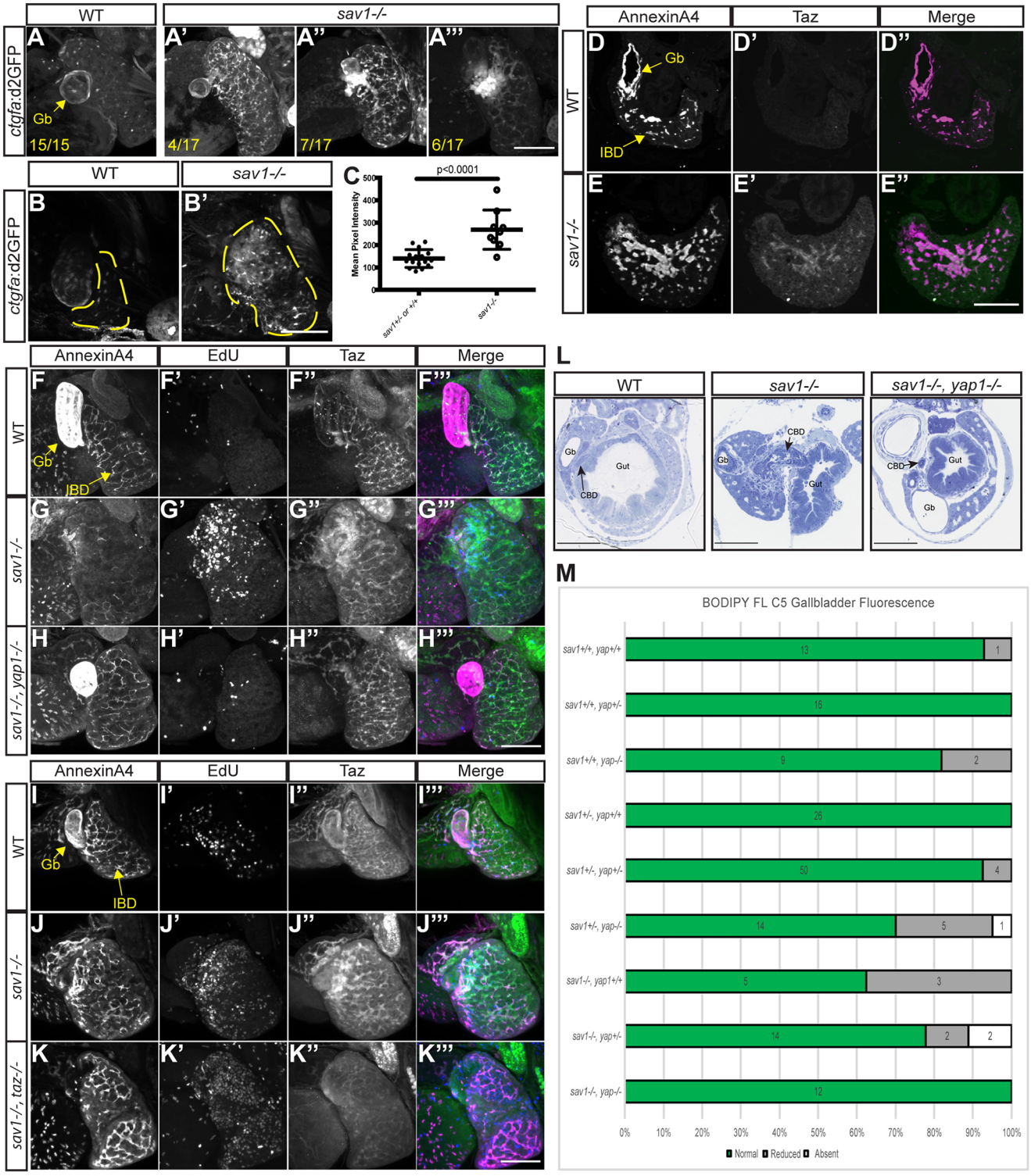

Fig. 4. Yap but not Taz drives *sav1*$^{-/-}$ phenotypes. (A-A‴) Whole-mount GFP staining of *ctgfa*:d2GFP wild-type and *sav1*$^{-/-}$ embryos. Gb, gallbladder. Numbers indicate the ratio of fish that displayed the phenotype/total fish analyzed. Scale bar: 100 µm. (B,B′) Images of *ctgfa*:d2GFP^{+} wild-type and *sav1*$^{-/-}$ larvae; dashed yellow line outlines the liver. Scale bar: 100 µm. (C) Mean pixel intensity of *ctgfa*:d2GFP reporter in livers as outlined in B: *n*=16 wild-type; *n*=9 *sav1*$^{-/-}$. Data are mean±s.d. Unpaired *t*-test with equal s.d. resulted in *P*<0.0001. (D-E″) Immunofluorescent staining of paraffin wax-embedded sections for Yap and Taz in *sav1*$^{-/-}$ and wild-type siblings, and colocalization with the biliary marker annexin A4. Gb, gallbladder; IBD, intrahepatic bile duct. Scale bar: 100 µm. (F-F‴) Whole-mount staining for annexin A4, EdU and Taz in wild-type larvae. Gb, gallbladder; IBD, intrahepatic bile duct. (G-G‴) Whole-mount analysis of *sav1*$^{-/-}$ larvae using the markers described in F (*n*=6). (H-H‴) Whole-mount analysis of *sav1*$^{-/-}$;*yap*$^{-/-}$ larvae using the markers described in F (*n*=8). Scale bar: 100 µm. (I-K‴) Repeated whole-mount analysis for the markers as described in F-H (although *n*=5 for *sav1*$^{-/-}$;*taz*$^{-/-}$ embryos). Scale bar: 100 µm. (L) Toluidine Blue stained sections of liver and gallbladder in wild-type, *sav1*$^{-/-}$ and *sav1*$^{-/-}$;*yap*$^{-/-}$ larvae at 10 dpf (*n*=9). Gb, gallbladder; CBD, common bile duct. *n*=7 wild type; *n*=5 *sav1*$^{-/-}$; *n*=4 *sav1*$^{-/-}$;*yap*$^{-/-}$. Scale bars: 100 µm. (M) Ratiometric analysis at 8 dpf of BODIPY FL C5 gallbladder uptake in larvae from a *sav1*$^{+/-}$;*yap*$^{+/-}$ incross. Analyses performed at 8 dpf unless otherwise indicated.

Development (2020) 147, dev184242. doi:10.1242/dev.184242

type embryos. The Yap and Taz antibody revealed staining throughout the liver, gallbladder, pancreas and gut without enrichment in biliary cells at both 80 hpf and 8 dpf (Fig. S5C-C″). In contrast, Taz staining is elevated in the biliary system with staining in intrahepatic biliary epithelial cells, common bile duct and gallbladder at both 80 and 8 dpf (Fig. S5A-A″, Fig. 4F-F‴). These differences suggest that Yap activity may be more broadly required across tissues, while Taz activity is more important in biliary epithelial cells. Analysis of Yap and Taz staining in *sav1*$^{-/-}$ fish with a severe phenotype showed increased Yap and Taz staining, with particularly high levels at the normal region of the gallbladder, when compared with wild-type siblings (Fig. S5E,F). Staining of Taz, in *sav1*$^{-/-}$ fish with severe phenotypes revealed similar results, although elevated expression was more restricted to the biliary system (Fig. S5E′,F′). These changes are not seen before the biliary phenotype manifests, as staining for Yap and Taz and Taz alone appears unaltered in *sav1*$^{-/-}$ larvae at 80 hpf (Fig. S5A-D″). Additional double staining of annexin A4 and Taz revealed increased Taz was associated with loss of annexin A4 staining, as well as annexin A4^{+} cells with abnormal morphology (Fig. 4G,G″). Staining on paraffin sections confirmed that *sav1*$^{-/-}$ fish had increased Taz within annexin A4^{+} biliary cells (Fig. 4D-E′). Elevated Taz staining was also associated with increased EdU incorporation, suggesting it may drive expansion of abnormal biliary epithelial cells (Fig. 4G′,G″). These results imply both Yap and Taz serve as important effectors of Hippo signaling and may drive the biliary phenotypes observed in *sav1*$^{-/-}$ larvae.

To directly test the roles of Yap and Taz in biliary cell development and maintenance, we generated *sav1*$^{-/-}$;*yap*$^{-/-}$ and *sav1*$^{-/-}$; *taz*$^{-/-}$ fish, and analyzed their effects on proliferation and biliary morphology. Deletion of *yap* in a *sav1*$^{-/-}$ mutant rescued the changes in EdU incorporation (Fig. 4F′,G′,H′). *sav1*$^{-/-}$;*yap*$^{-/-}$ mutants also rescue abnormal biliary morphology assessed by histology and marker analysis (Fig. 4F-H,L). The abnormal morphology and loss of gallbladder was also rescued, as seen using BODIPY FL C5 fluorescence (Fig. 4M). Surprisingly, there was no change in either phenotype of *sav1*$^{-/-}$;*taz*$^{-/-}$ fish when compared with *sav1*$^{-/-}$ mutants alone, despite the enriched expression of Taz in the biliary system (Fig. 4I-K‴). Together, these results suggest that elevated Yap is primarily responsible for the ductal phenotypes observed in *sav1*$^{-/-}$ mutant zebrafish. Although additional loss of *yap* in *sav1* mutants rescued all phenotypes at 8 dpf, it did not rescue the lethality of the *sav1* mutants. One possible explanation for this could be an essential role in maintaining appropriate Taz levels at post-larval stages.

Hippo signaling in hepatocytes is crucial for gallbladder and biliary development

The broad expression of Yap and Taz throughout the hepatopancreatic ductal system has important implications on the biliary phenotypes of *sav1*$^{-/-}$ mutants. In particular, Yap and Taz expression suggests the possibility that Hippo signaling affects biliary development both cell-autonomously and non-autonomously. A likely candidate for non-autonomous signaling to biliary cells is the adjacent hepatocyte population. To test whether Hippo signaling in hepatocytes may affect the adjacent biliary system, we re-expressed Sav1 in the hepatocytes of *sav1*$^{-/-}$ embryos using the −2.8 kb *lfabp* (Her et al., 2003). This promoter is active in hepatocytes, but not in annexin A4^{+} biliary cells (Wilkins et al., 2014). Embryos expressing the transgene *lfabp:* eGFP-2a:Sav1 were analyzed and compared with non-transgenic siblings. Surprisingly, hepatocyte-specific re-expression of Sav1 protein in *sav1*$^{-/-}$ fish rescued both the loss of gallbladder and the abnormal biliary morphology of non-transgenic *sav1*$^{-/-}$ siblings. This was true for all embryos analyzed at both 8 and 16 dpf (Fig. 5C-H). The *lfabp* promoter is not active in the gallbladder, even at the earliest points of development in either wild-type or mutant larvae (Fig. 5A,B). These results suggest that Hippo activity within hepatocytes has important non-autonomous impact on gallbladder and biliary cell development.

Hepatocyte morphology and polarity are altered in *sav1* mutants

We assessed hepatocyte morphology by histology and TEM. Low magnification of tissue sections did not indicate changes to hepatocytes at 10 dpf. However, ultra-structural analysis by TEM revealed defects in bile duct canaliculi. Although we regularly identified canaliculi in wild-type fish, we were often unable to identify these structures in *sav1*$^{-/-}$ sibling fish (Fig. 6A-B″). The rare canaliculi in *sav1*$^{-/-}$ fish appeared shorter and wider than those of wild-type siblings (Fig. 6C,D). In mutant fish without clear canaliculi, we observed excessive membranous material at hepatocyte-biliary contacts, where tight junctions could not be identified (Fig. 6B,B′). We also noted expanded extracellular space between intrahepatic biliary cells and adjacent hepatocytes (Fig. 6B″). This space was filled with amorphous material of varying electron densities and may represent improper secretion of bile. These results suggest that hepatocyte polarity is altered in *sav1*$^{-/-}$ fish; specifically, the apical domain may be expanded, and canaliculi improperly formed.

The bile duct canaliculi are formed by the specialized apical domains of hepatocytes, which contact adjacent biliary cells forming tight junctions. To further assess hepatocyte polarity, we performed immunofluorescent staining for Alcam, which becomes restricted to apical membranes of hepatocytes after apicobasal polarity is established (Sakaguchi et al., 2008). In wild-type larvae at 8 dpf, Alcam outlines the intrahepatic biliary system located adjacent to the apical domain of hepatocytes (Fig. 7A). Staining in *sav1*$^{-/-}$ siblings reveals a similar phenotypic spectrum to that produced by annexin A4 immunoreactivity. Across this spectrum, Alcam is expanded, suggesting enlargement of the apical domain (Fig. 7B-B‴). In contrast to annexin A4 staining, the most severe mutants never lose Alcam staining, but instead show expansion throughout the liver (Fig. 7B‴).

We also stained for apical domain marker atypical protein kinase C (aPKC). In wild-type larvae, aPKC labels the apical canalicular membrane of hepatocytes, whereas in *sav1*$^{-/-}$ siblings these structures are lost and instead staining is expanded around the periphery of hepatocytes, suggesting a loss of proper apicobasal polarity (Fig. 7C-D″). These changes develop concurrently with those observed in the biliary epithelial cells, as shown by annexin A4 staining, with the most severe annexin A4 phenotypes corresponding to peripheral expansion and canalicular loss of aPKC (Fig. 7G-J). aPKC staining also marked the apical domains of the epithelial cells of the gallbladder, and illustrates morphological changes in the gallbladder, suggesting these cells may also lose proper polarity (Fig. 7E-F″).

To further assess hepatocyte morphology, we stained for cadherin 2 (Cdh2). In wild-type larvae, Cdh2 labels the cadherin junctions between hepatocytes, marking the periphery of hepatocytes (Fig. 7K-K″). Although hepatocyte shape did not appear significantly altered in *sav1*$^{-/-}$ larvae, we found that as the annexin A4 phenotype increased in severity, Cdh2 staining diminished

Development (2020) 147, dev184242. doi:10.1242/dev.184242

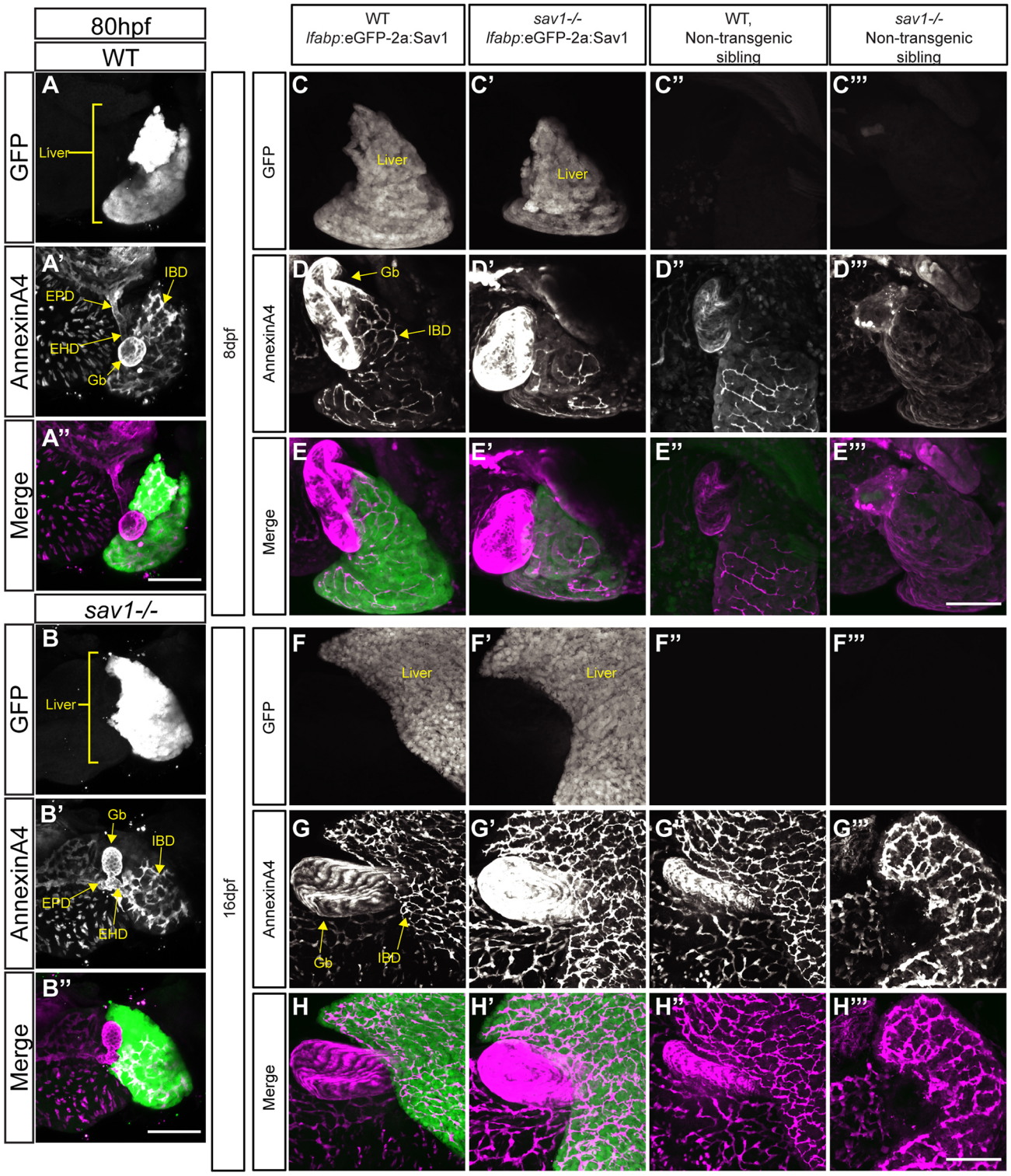

Fig. 5. Hepatocyte Hippo signaling is crucial for larval survival and functions non-cell-autonomously to affect the intrahepatic and extrahepatic biliary system. (A,B,C-C‴,F-F‴) Whole-mount GFP staining in wild-type and *sav1*$^{-/-}$ larvae. (A′,B′,D-D‴,G-G‴) Annexin A4 staining of gallbladder and intrahepatic biliary cells. Gb, gallbladder; EHD, extrahepatic duct; EPD, extrapancreatic duct; IBD, intrahepatic bile duct. (A″,B″,E-E‴,H-H‴) Merged images with green representing GFP and magenta representing annexin A4. (A-B″) Larvae at 80 hpf (*n*=3 wild type, *lfabp:*eGFP-2a:Sav1+ and *sav1*$^{-/-}$, *lfabp:*eGFP-2a:Sav1+). (C-E‴) Larvae at 8 dpf (*n*=8 wild type, *lfabp:*eGFP-2a:Sav1+; *n*=7 *sav1*$^{-/-}$, *lfabp:*eGFP-2a:Sav1+; *n*=3 wild type, non-transgenic sibling; *n*=5 *sav1*$^{-/-}$, non-transgenic sibling). (F-H‴) Fish at 16 dpf (*n*=12 wild type, *lfabp:*eGFP-2a:Sav1+; *n*=12 *sav1*$^{-/-}$, *lfabp:*eGFP-2a:Sav1+; *n*=8 wild type, non-transgenic sibling; *n*=4 *sav1*$^{-/-}$, non-transgenic sibling). Scale bars: 100 µm.

and, in the most severe mutants, sporadic hepatocytes displayed bright cytoplasmic Cdh2 staining, suggesting collapse of cadherin junctions (Fig. 7L-N).

Together, these results reveal that hepatocytes in *sav1*$^{-/-}$ larvae lose proper morphology, polarity and cell-cell junctions. As proper hepatocyte polarity and junction formation is essential for proper

Development (2020) 147, dev184242. doi:10.1242/dev.184242

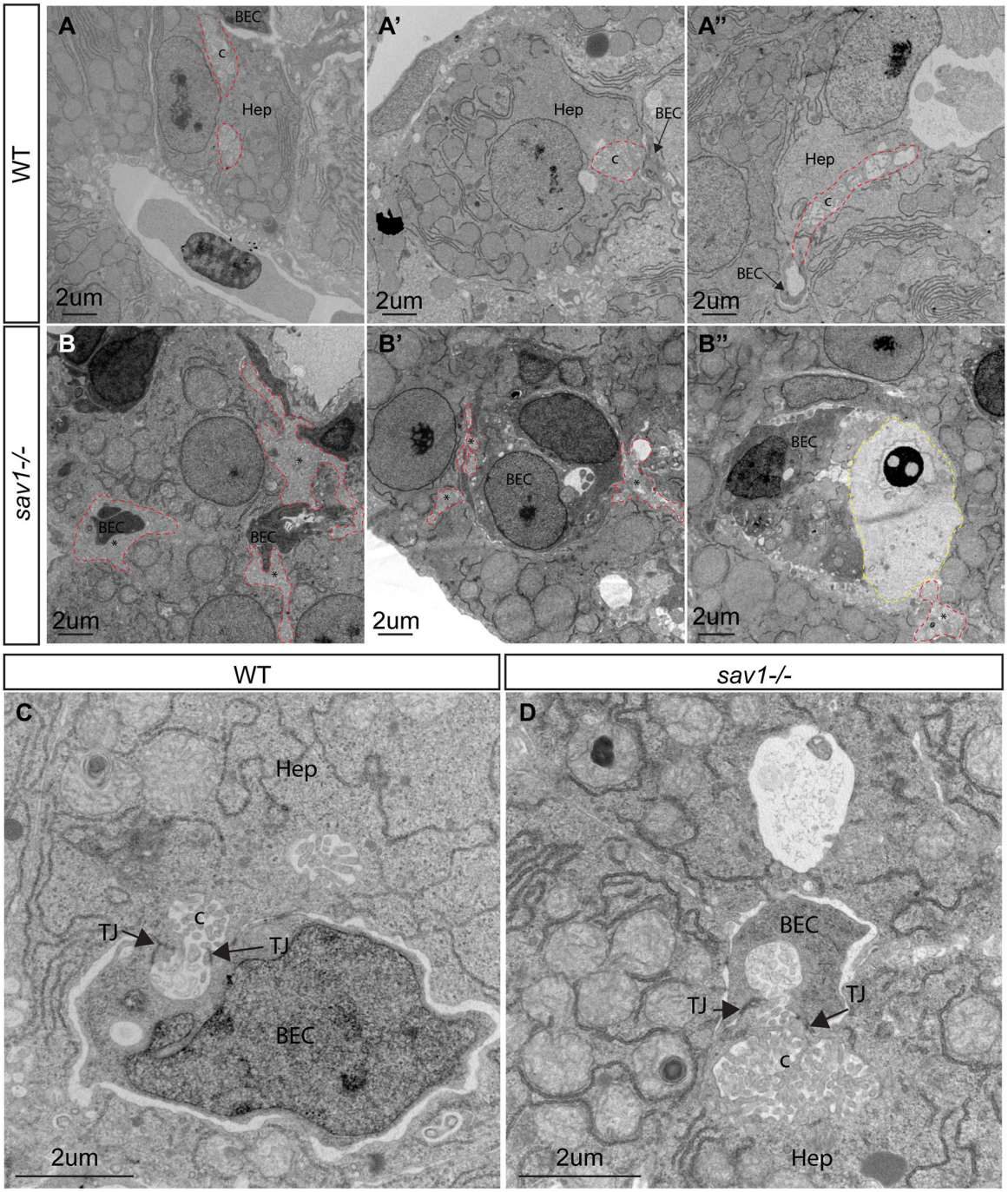

Fig. 6. Ultrastructural defects of bile duct canaliculi in *sav1*$^{-/-}$ larvae. (A-A″) TEM examples of wild-type canaliculi and hepatocyte-biliary epithelial cell junctions. Canaliculi are outlined with dashed red lines. (B-B″) *sav1*$^{-/-}$ siblings of A-A″ showing examples of hepatocyte-to-biliary cell borders that contain membranous material reminiscent of canaliculi, but lack normal structure (dashed red lines). In B″, a dashed yellow line outlines excessive extracellular space filled with electron-dense material. (C) Higher magnification of wild-type hepatocyte-biliary epithelial cell junction and canaliculi. (D) Example of a rare canaliculi present in *sav1*$^{-/-}$ larvae showing shorter length and increased diameter. Hep, hepatocyte; BEC, biliary epithelial cell; c, canaliculi; TJ, tight junction. Asterisks indicate abnormal canaliculi or abnormal hepatocyte membrane. *n*=3 wild type, *n*=3 *sav1*$^{-/-}$. All images are of 10 dpf larvae.

bile secretion, these results suggest hepatocyte function is also altered.

Non-hepatocyte Hippo signaling is required for maintenance of the gallbladder and extrahepatic biliary ducts

Strikingly, hepatocyte-specific expression of Sav1 allowed *sav1*$^{-/-}$ fish to survive to adulthood. Observing the transgenic fish, we noticed that *sav1*$^{-/-}$ mutants were significantly reduced in size when compared with wild-type siblings that also expressed the *lfabp:*eGFP-2a:Sav1 transgene (Fig. S6A,B). Upon dissection and closer analysis of *sav1*$^{-/-}$ fish, we were unable to identify gallbladders in any surviving adults. Instead, we saw cells continuous with adjacent liver tissue in the anticipated gallbladder region but lacking GFP expression (Fig. S6C-C″). Whole-mount immunostaining revealed that, although these structures were devoid of *lfabp:*eGFP-2a:Sav1 expression, they showed staining of biliary marker annexin A4,

Development (2020) 147, dev184242. doi:10.1242/dev.184242

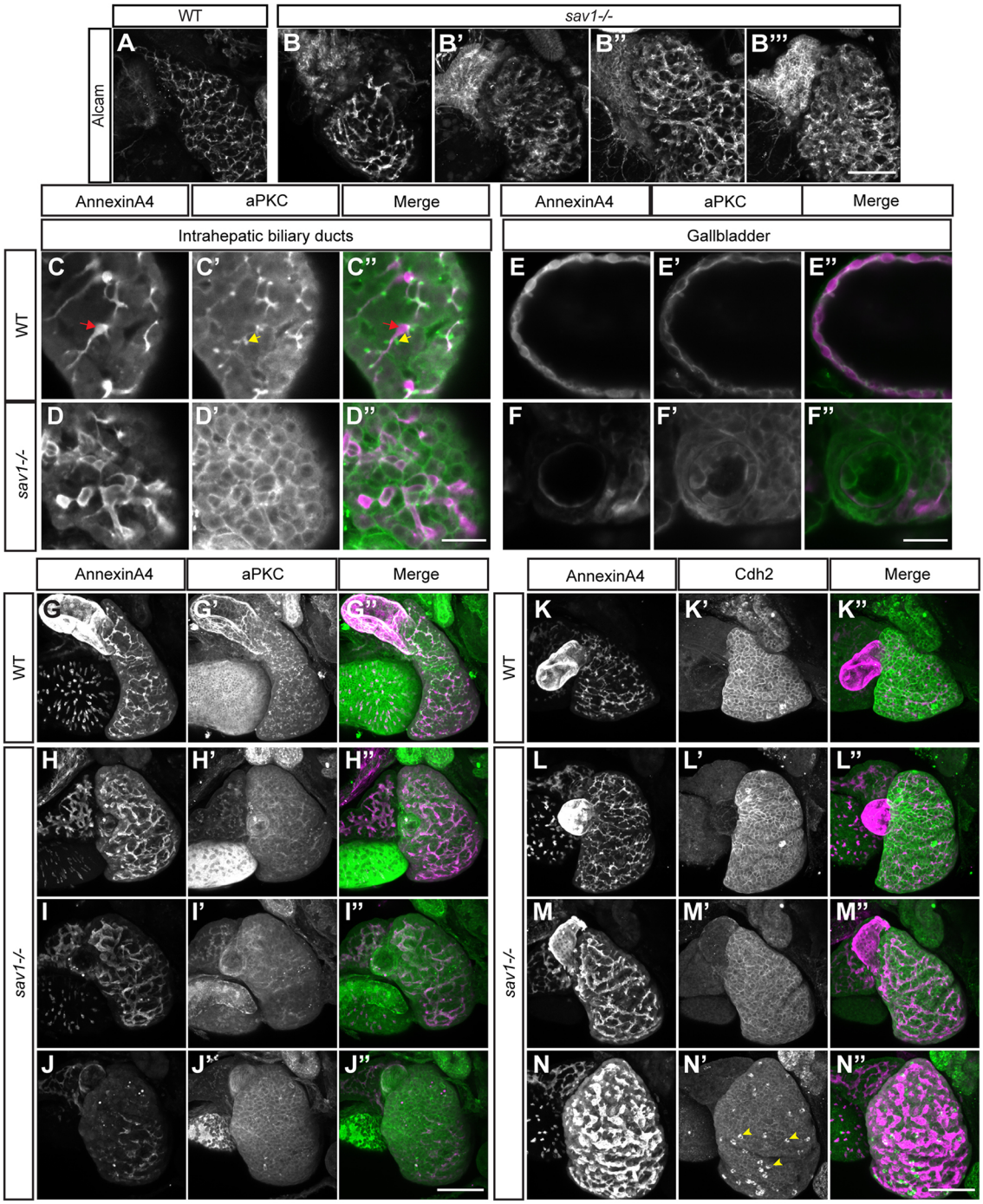

Fig. 7. Hepatocyte apical domains appear abnormal and expanded in *sav1*$^{-/-}$ larvae. (A-B‴) Examples of wild-type (A) and *sav1*$^{-/-}$ (B-B‴) 8 dpf larvae whole-mount immunostaining for Alcam. *n*=5 wild type, *n*=6 *sav1*$^{-/-}$. Scale bar: 100 µm. (C,D) Single plane images of intrahepatic biliary ducts stained for annexin A4 in wild-type and *sav1*$^{-/-}$ 8 dpf larvae respectively. Red arrow in C indicates one annexin A4^{+} biliary epithelial cell. (C′,D′) Single plane images of aPKC staining in wild-type and *sav1*$^{-/-}$ 8 dpf larvae, respectively. Yellow arrow in C′ indicates one canaliculus. (C″,D″) Merged images with green representing aPKC and magenta representing annexin A4. Scale bar: 25 µm. (E-F″) Examples of wild-type and *sav1*$^{-/-}$ gallbladder stained for aPKC and annexin A4, following the same labeling conventions as in C-D″. (G,G′) *Z*-projections of whole-mount staining for annexin A4 and aPKC in wild-type larvae at 8 dpf. Scale bar: 25 µm. (H,H′,I,I′,J,J′) *Z*-projections of whole-mount staining for annexin A4 and aPKC in *sav1*$^{-/-}$ larvae at 8 dpf. (G″,H″,I″,J″) Merged images with green representing aPKC and magenta representing annexin A4 (*n*=7 wild type; *n*=5 *sav1*$^{-/-}$). Scale bar: 100 µm. (K-K″) *Z*-projections of whole-mount staining for annexin A4 and Cdh2 in wild-type larvae at 8 dpf. (L,L′,M,M′,N,N′) *Z*-projections of whole-mount staining for annexin A4 and Cdh2 in *sav1*$^{-/-}$ larvae at 8 dpf. Yellow arrowheads in N′ indicate examples of high intensity cytoplasmic punctate Cdh2 staining, suggesting cadherin junction collapse. (L″,M″,N″) Merged images of Cdh2 (green) and annexin A4 (magenta) (*n*=7 wild type; *n*=6 *sav1*$^{-/-}$). Scale bar: 100 µm.

suggesting these cell clusters might be biliary duct carcinomas (Fig. 8A-C‴). Hematoxylin and Eosin histology, and annexin A4 immunoreactivity confirmed a cholangiocarcinoma-like identity (Fig. 8D-E′,F′,I′). Further staining revealed that both these biliary cells and the surrounding tissue were positive for Yap and Taz, suggesting they may drive the formation of these masses (Fig. 8G′,J′).

Development (2020) 147, dev184242. doi:10.1242/dev.184242

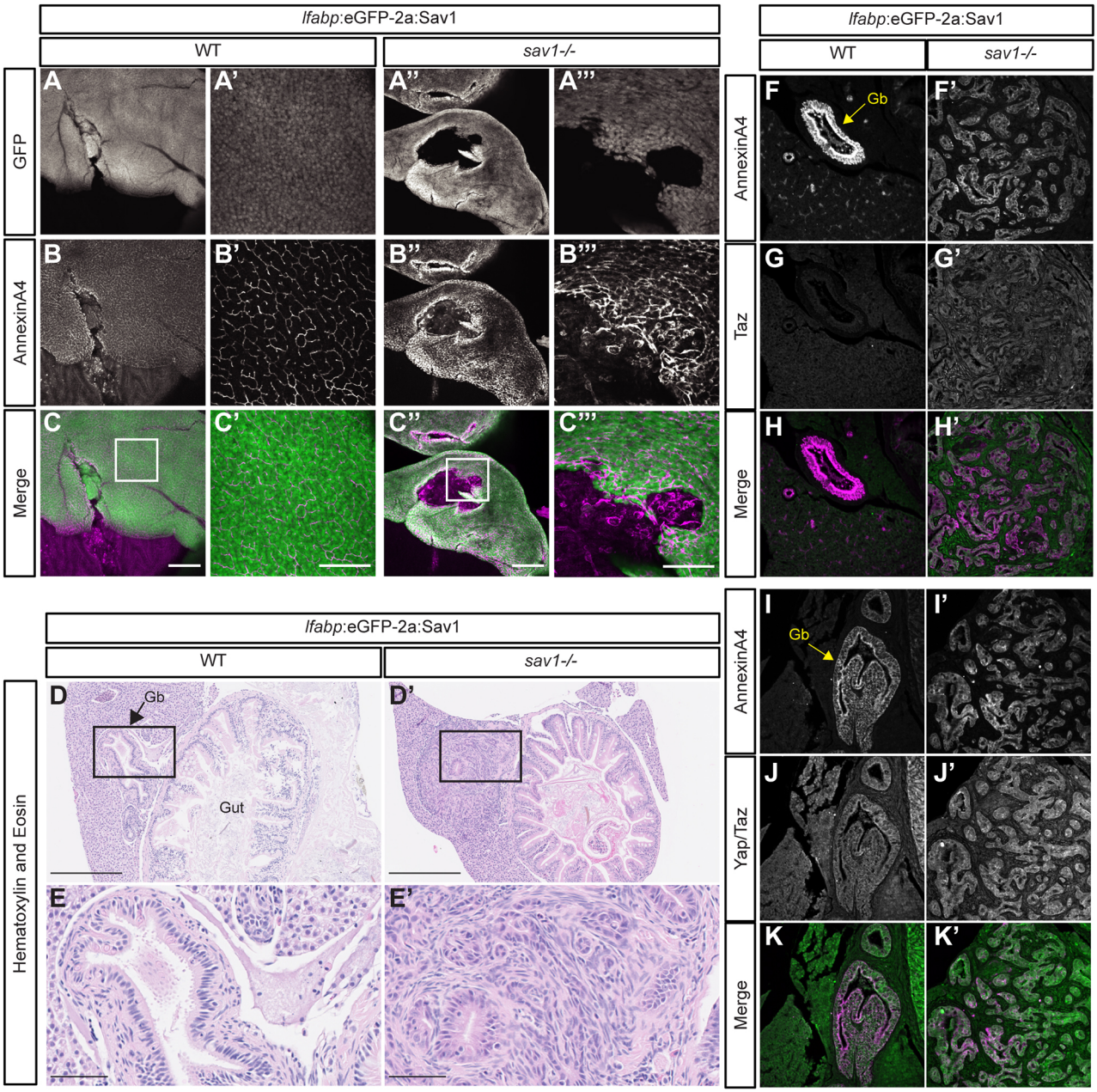

Fig. 8. Hippo signaling functions cell-autonomously in the maintenance of the gallbladder and extrahepatic biliary ducts. (A-A‴) Whole-mount GFP staining in wild-type and *sav1*$^{-/-}$ adult fish. (B-B‴) Whole-mount annexin A4 staining in wild-type and *sav1*$^{-/-}$ adult fish. (C-C‴) Merged images of GFP (green) and annexin A4 (magenta). Scale bars: 250 µm in C,C″; 100 µm in C′,C‴. (D-E′) Hematoxylin and Eosin histology of the same fish analyzed in A-C‴. Gb, gallbladder (*n*=10 wild type, *lfabp:*eGFP-2a:Sav1+; *n*=8 *sav1*$^{-/-}$, *lfabp:*eGFP-2a:Sav1+). Scale bars: 250 µm in D and E; 50 µm in D′ and E′. (F,F′,I,I′) Annexin A4 immunostaining on wild-type and *sav1*$^{-/-}$ dissected liver and gut of fish carrying *lfabp:*eGFP-2a:Sav1 transgene. Gb, gallbladder. (G,G′) Taz staining on the same sections shown in F,F′. (J,J′) Yap and Taz staining on the same sections shown in I,I′. (H,H′,K,K′) Merged images of Taz alone, Yap and Taz (green), and annexin A4 (magenta) (*n*=5 wild type, *lfabp*:eGFP-2a:Sav1+, *n*=3 *sav1*$^{-/-}$, *lfabp:*eGFP-2a:Sav1+).

These results suggested core Hippo pathway components may be altered in human biliary carcinoma, particularly in extrahepatic cases. Indeed, analysis of cBioportal data is consistent with this possibility (Fig. S7; Table S1) (Cerami et al., 2012; Gao et al., 2013). The eventual loss of gallbladder in *sav1*$^{-/-}$, *lfabp:*eGFP-2a:Sav1 adults reveals a previously unrecognized role for Hippo signaling in the extrahepatic biliary network, consistent with data from larval zebrafish.

stk3 mutants phenocopy *sav1* mutants with delayed onset

Sav1 has been shown to primarily affect Yap and Taz through the Hippo kinases Mst1 and Mst2. To assess whether the gallbladder and biliary phenotypes found in *sav1*$^{-/-}$ zebrafish depend on canonical Hippo signaling, we targeted *stk3* for mutation, as it encodes Stk3, the only known ortholog of Mst1 and Mst2 present in zebrafish. Using transcription activator-like effector nucleases (TALENs), we generated a 5 bp deletion early in exon2 of *stk3*. This deletion causes a nonsense frameshift mutation leading to a premature stop codon early in *stk3* before any known functional domains (Fig. 9A). Stk3 was undetectable in western blot extracts of 8 dpf *stk3*$^{-/-}$ fish, confirming the mutant allele leads to loss of protein (Fig. 9B). Lack of Stk3 causes larval lethality with loss of Mendelian ratios first appearing at 16 dpf and no mutants recovered

Development (2020) 147, dev184242. doi:10.1242/dev.184242

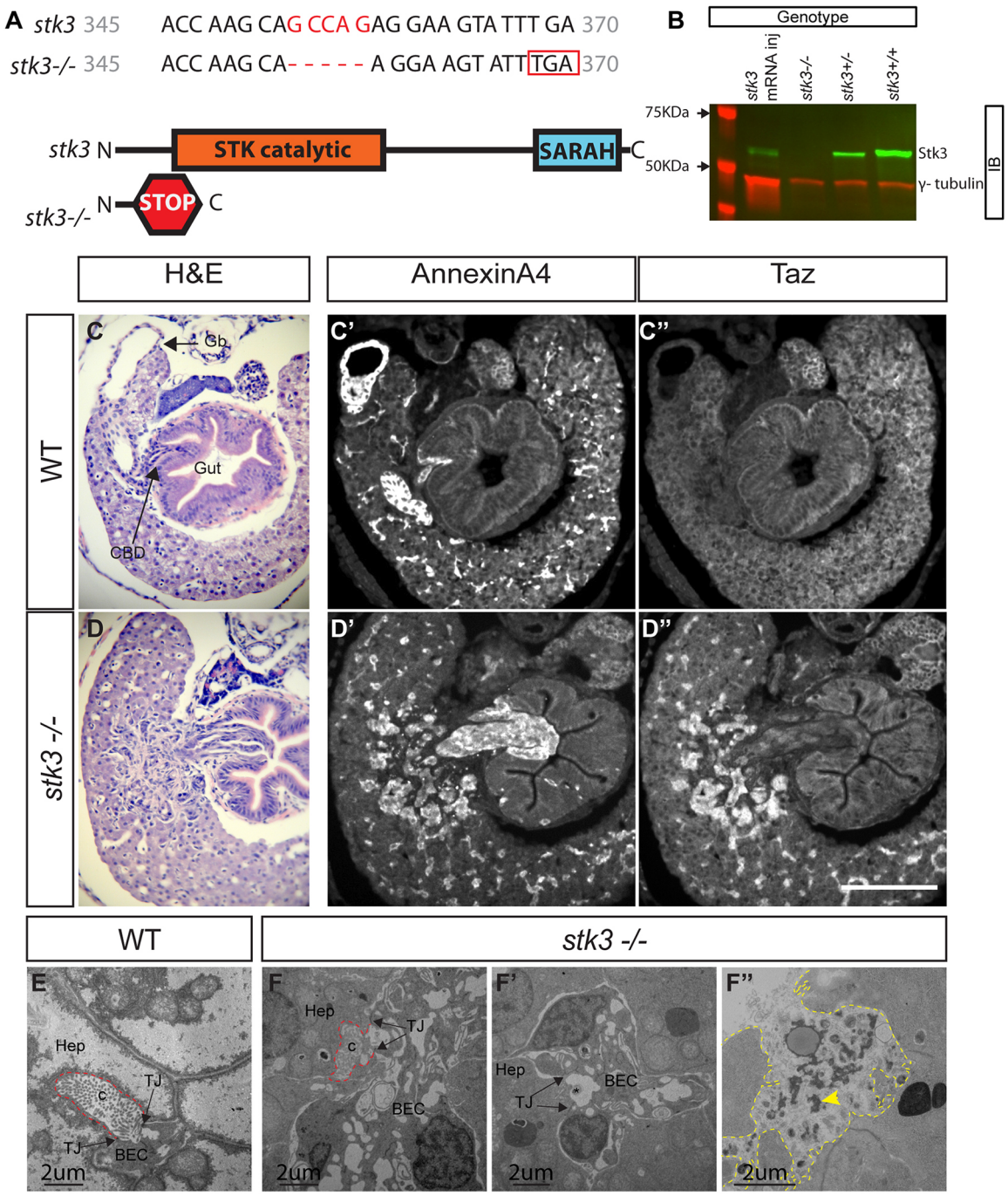

Fig. 9. *stk3* mutants phenocopy *sav1* mutants, but with delayed onset. (A) Schematic depicting wild-type and mutant alleles of zebrafish *stk3*. *stk3* mutant alleles contain a 5 bp deletion (red), causing a frameshift and early stop codon (red box). (B) Western blot of protein lysates from *stk3*$^{-/-}$, *stk3*$^{+/-}$ and *stk3*$^{+/+}$ single larvae at 8 dpf. γ-Tubulin staining was used as a loading control. (C-D″) Paraffin histology shows abnormal biliary cells with increased Yap and Taz levels using immunofluorescent and Hematoxylin and Eosin staining in *stk3*$^{-/-}$ fish at 16 dpf compared with wild-type siblings. Gb, gallbladder; CBD, common bile duct (*n*=5 wild type; *n*=5 *stk3*$^{-/-}$). Scale bar: 100 µm. (E) TEM example of wild-type canaliculi and hepatocyte-biliary epithelial cell junctions. Canaliculi are outlined with dashed red lines. (F-F′) *stk3*$^{-/-}$ siblings of E showing examples of abnormal canaliculi, with shorter abnormal shape (F) or no canalicular structure despite tight junctions connecting the hepatocyte to the adjacent biliary epithelial cell (F′). These areas are outlined with dashed red lines and/or labeled with an asterisk for possible canaliculi with abnormal structure. (F″) A dashed yellow line outlines excessive extracellular space filled with electron-dense material. Yellow arrowhead indicates bile salt deposit. Hep, hepatocyte; BEC, biliary epithelial cell; c, canaliculi; TJ, tight junction (*n*=3 wild type; *n*=3 *stk3*$^{-/-}$). All images are of 16 dpf larvae.

beyond 28 dpf. Histology revealed similar morphology changes as seen in *sav1*$^{-/-}$ larvae. Specifically, we found abnormal gallbladder as well as intra- and extrahepatic biliary ducts by examining Hematoxylin and Eosin stained sections (Fig. 9C″,D″). However, these changes were first visible at 16 dpf, notably later than the 7 dpf phenotypic onset of *sav1*$^{-/-}$ larvae. Immunostaining of adjacent sections confirmed the abnormal morphology of biliary epithelial cells with increased Yap and Taz levels (Fig. 9C-D′). Similar to *sav1*$^{-/-}$ mutants, TEM of *stk3*$^{-/-}$ larvae revealed that bile duct canaliculi were rarely detected, and those that were identified

Development (2020) 147, dev184242. doi:10.1242/dev.184242

appeared dysplastic (Fig. 9E-F′). We also observed amorphous electron-dense material, likely bile salts, in expanded extracellular spaces (Fig. 9F″). Additional deletion of *yap* in *stk3* larvae rescued this abnormal morphology (Fig. S8A-C). Similar to *sav1*$^{-/-}$;*yap*$^{-/-}$ fish, abrogation of Yap in *stk3*$^{-/-}$ mutants did not rescue larval lethality. These results led us to conclude that *stk3* mutants phenocopy *sav1* mutants, but exhibit delayed onset. Delayed phenotype onset may be due to partially redundant kinase(s) functioning in the Hippo signaling cascade.

Phosphatase PP2A plays an inhibitory role in zebrafish Hippo signaling

Since the Hippo signaling pathway was first described, Sav1 has been recognized as promoting the activation of the core kinase cascade. However, the molecular mechanisms behind activation are still being elucidated. Recently, through *in vitro* protein interaction assays, Sav1 has been shown to promote Stk3 activation through inhibition of the PP2A phosphatase complex (Bae et al., 2017). We sought to test the role of this phosphatase *in vivo* and in the context of Yap activity within the liver. We reasoned the delayed phenotypic onset in *stk3*$^{-/-}$ larvae could be explained by the presence of a redundant kinase also regulated by Sav1 and the PP2A phosphatase complex. To test whether this phosphatase complex functions in zebrafish we used the PP2A inhibitor, LB-100 (Lu et al., 2009; Hong et al., 2015). Larvae from multiple *sav1*$^{+/-}$ in-crosses were treated with 20 µM LB-100 or vehicle (PBS) every 48 h, starting at 60 hpf and ending at 180 hpf. All fish were then imaged by confocal microscopy and assessed for *ctgfa:d2GFP* fluorescence intensity throughout the liver (Fig. 10A). After collecting images and recording pixel intensity, fish were then genotyped. *sav1*$^{-/-}$ larvae treated with PBS vehicle displayed increased fluorescence intensity compared with wild-type siblings as previously measured. However, *sav1*$^{-/-}$ larvae treated with LB-100 showed statistically indistinguishable levels from wild-type vehicle-treated siblings, and significantly lower fluorescence levels compared with vehicle-treated *sav1*$^{-/-}$ siblings (Fig. 10B-D). To determine whether the morphological defects seen in *sav1*$^{-/-}$ larvae were also rescued, we assessed LB-100 *sav1*$^{-/-}$ larvae for the presence of morphologically normal gallbladders. We found that although 9/18 PBS-treated larvae displayed abnormal or unrecognizable gallbladder morphology, only 2/19 LB-100 treated siblings exhibited such defects. These results show inhibition of PP2A decreased a readout of Yap and Taz transcriptional activity and partially rescued the morphological defects seen in *sav1*$^{-/-}$ larvae, suggesting that Sav1 indeed activates Stk3 through inhibition of the PP2A phosphatase complex *in vivo*, in a physiologically relevant context (Fig. 10E).

sav1 and *stk3* display a synergistic genetic interaction

Based on the above results, we hypothesized that loss of *sav1* led to inhibition of both Stk3 as well as an unidentified redundant kinase. To further test this hypothesis, we generated *sav1*$^{-/-}$; *stk3*$^{-/-}$ fish and examined them at 7 and 10 dpf. If a redundant kinase was responsible for the difference between *sav1*$^{-/-}$ and *stk3*$^{-/-}$ phenotype onset, then *sav1*$^{-/-}$; *stk3*$^{-/-}$ embryos should phenocopy their *sav1*$^{-/-}$ siblings. *sav1*$^{-/-}$; *stk3*$^{-/-}$ fish also displayed absent or abnormal gallbladders, similar to *sav1*$^{-/-}$ fish, when assessed by histology at both 7 and 10 dpf (Fig. 11A-D′). However, the abnormal ductal cell morphology was significantly more severe in *sav1*$^{-/-}$; *stk3*$^{-/-}$ fish compared with *sav1*$^{-/-}$ siblings (Fig. 11A-D′); this was especially apparent when assessing cellular morphology by TEM (Fig. 11F). Supporting this synergistic genetic interaction, we were unable to recover any *sav1*$^{-/-}$; *stk3*$^{-/-}$ mutants at 16 dpf, whereas both *sav1*$^{-/-}$ and *stk3*$^{-/-}$ single mutants survived and were recovered at this time-point. BODIPY FL C5-ceramide gallbladder uptake again reinforced this genetic interaction (Fig. 11E). In addition, proximal renal tubules in *sav1*$^{-/-}$; *stk3*$^{-/-}$ double mutants displayed abnormal cell morphology at 10 dpf, as they appeared dilated and fibrotic (Fig. 11G,H). This phenotype was fully penetrant in *sav1*$^{-/-}$; *stk3*$^{-/-}$ double mutants at 10 dpf, while only rarely seen in *sav1*$^{-/-}$ single mutants at 21 dpf. These results suggest a role for *sav1* outside of its known canonical kinase activation in Hippo signaling.

DISCUSSION

Non-cell autonomous signaling from hepatocytes to the extrahepatic biliary ducts

There are several significant conclusions from our investigations. Perhaps the most intriguing and novel result is the rescue of both intra- and extrahepatic defects by re-expression of Sav1 in hepatocytes, suggesting signaling from hepatocytes to the developing gallbladder. Although we have not identified the mechanisms behind this signaling, we discuss a possibility.

We hypothesize that bile secretion from hepatocytes into the intrahepatic ducts, extrahepatic ducts and the gallbladder is necessary for delivering proper paracrine signals required for extrahepatic biliary development and maintenance. As bile from hepatocytes contacts each of these cell types, it is a probable method for signaling between these tissues. Although bile salts are well known for their role in fat digestion and absorption, they can also act as signaling molecules. The biliary tree expresses several bile acid receptors. Nuclear receptors farnesoid X receptor (FXR) and vitamin D receptor (VDR) are activated by primary and secondary bile salts, and expressed in hepatocytes and cholangiocytes, respectively. Cholangiocytes also express several G-protein-coupled receptors responsive to bile salts, including sphingosine-1-phosphate receptor 2 (S1PR2) and Takeda G-couple protein receptor 5 (TGR5), which are localized at the apical membrane. The activation of these proteins is associated with a number of cell processes, including secretion, tight junction integrity, migration and proliferation (Deutschmann et al., 2018; Martinot et al., 2017). We found *sav1*$^{-/-}$ hepatocyte polarity and morphology is altered, suggesting proper secretion of bile salts may also be affected. Interestingly, the phenotype onset in *sav1*$^{-/-}$ fish coincides with initial feeding behavior and bile secretion. We reason that impaired secretion from hepatocytes due to altered polarity or maturation of hepatocytes may impact bile-mediated paracrine signals, leading to the intrahepatic and extrahepatic biliary defects in *sav1*$^{-/-}$ mutants. Exposure to physiologically relevant levels of bile acids activates Yap transcriptional programs in biliary epithelial cells (Pepe-Mooney et al., 2019). Recent work has also demonstrated that bile acid load within the bile canalicular network affects Yap localization in hepatocytes through the actomyosin cytoskeleton (Meyer et al., 2020). This study sets up the bile canalicular network as a signaling hub that affects Yap in hepatocytes; we hypothesize it could act similarly in biliary cells.

A complex role for Hippo signaling in hepatocytes

Notably, *sav1*$^{-/-}$ mutants were able to survive to adulthood only after re-expression of Sav1 in hepatocytes, suggesting that improper liver development, and perhaps subsequent liver failure is the cause of death in *sav1*$^{-/-}$ larvae. This is not entirely unexpected, as Hippo pathway components have been well documented as important regulators of Yap and as being required for hepatocyte differentiation (Camargo et al., 2007; Lee et al., 2016; Wu et al., 2017; Yimlamai et al., 2014). From EdU incorporation analysis, we

Development (2020) 147, dev184242. doi:10.1242/dev.184242

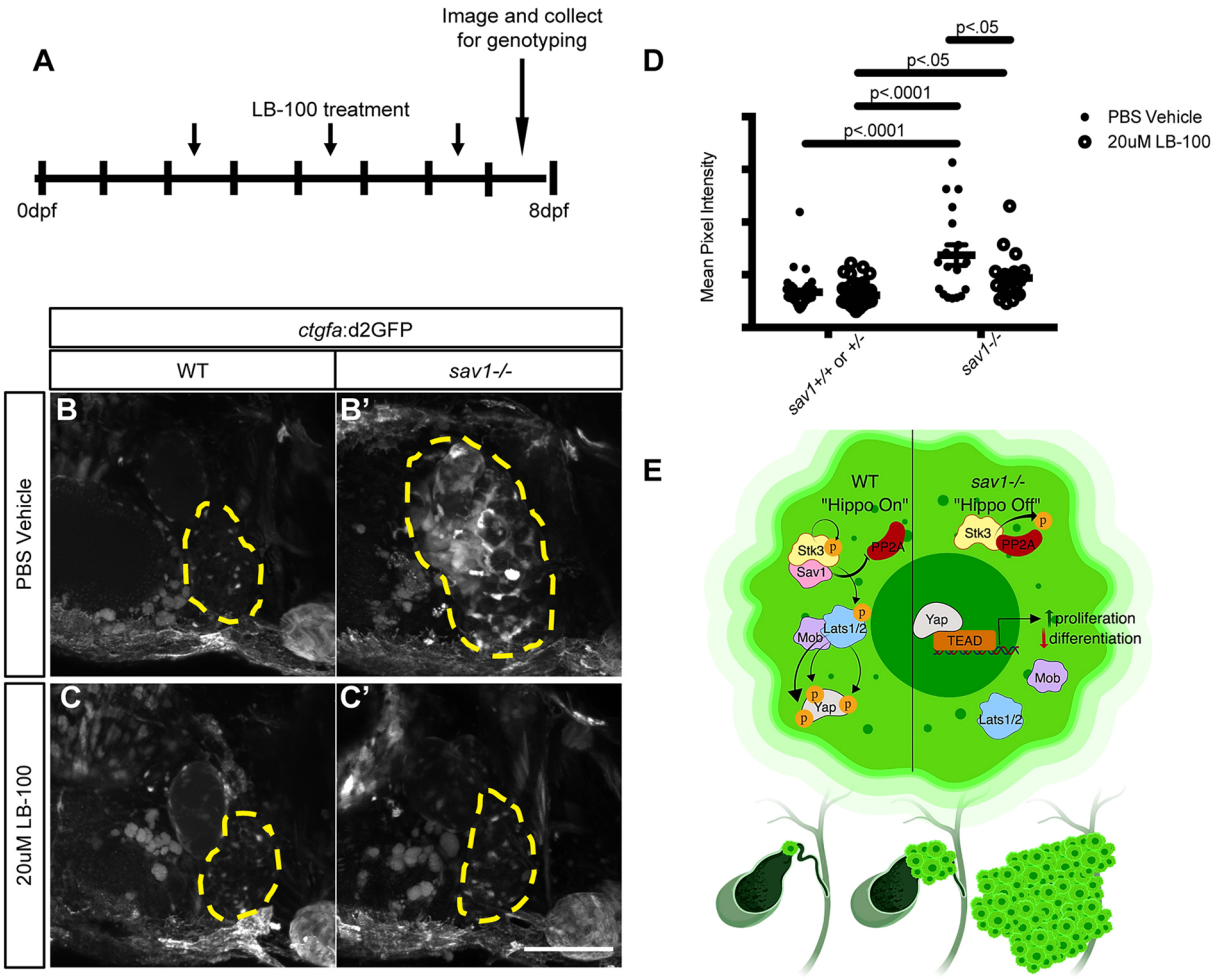

Fig. 10. Phosphatase PP2A plays an inhibitory role in zebrafish Hippo signaling. (A) Schematic of LB100 treatment. (B-C′) Images of *ctgfa:*d2GFP+ wild-type and *sav1*$^{-/-}$ larvae at 7 dpf, treated with PBS or 20 µM LB100; liver is indicated by a dashed yellow line. Scale bar: 100 µm. (D) Mean pixel intensity of *ctgfa:*d2GFP reporter in livers, as outlined in B. Data are mean±s.d. Two-way ANOVA with Tukey's multiple comparisons, *P* values are as indicated. PBS *sav1*$^{+/+}$ or *sav1*$^{+/-}$, *n*=42; PBS *sav1*$^{-/-}$, *n*=18; 20 µM LB100 *sav1*$^{+/+}$ or *sav1*$^{+/-}$, *n*=41; 20 µM LB100 *sav1*$^{-/-}$, *n*=18. (E) Model for PP2A function in Hippo pathway signaling of the biliary system.

noted that hepatocytes likely represent a proportion of the positive liver cells, as EdU uptake was not restricted to annexin A4^{+} biliary cells. Furthermore, overexpression of active Yap in zebrafish stimulates nucleotide biosynthesis, causes hepatomegaly and increases tumor susceptibility (Cox et al., 2016). Analysis of *yap*$^{-/-}$ zebrafish revealed impaired liver growth due to defects in glucose transport and nucleotide synthesis (Cox et al., 2018). Given the results of that study, it may be interesting to examine whether Yap-mediated nutrient regulation extends to the biliary system, particularly in the context of cholangiocarcinoma.

Hippo signaling in the intrahepatic biliary system

In addition to confirming previous findings from conditional mouse knockouts, our analysis in zebrafish provides new information for Hippo signaling in biliary cell biology. Our results indicating expansion of abnormal intrahepatic biliary cells are consistent with previous findings in mouse conditional knockouts of Hippo pathway components using *Alb*-Cre (Camargo et al., 2007; Wu et al., 2017; Zhang et al., 2010). However, as this Cre is not expressed in mature biliary epithelial cells, dysgenesis was due to defects in the bipotent liver progenitor cells and hepatocytes. Interestingly, we observed normal formation of intrahepatic biliary cells initially in global *sav1*$^{-/-}$ mutants, followed by development of abnormal morphology, increased proliferation and loss of the biliary cell marker annexin A4. These data suggest that Hippo signaling is also required in mature intrahepatic biliary cells for regulation of Yap. The rescue of intrahepatic defects by re-expression of Sav1 in hepatocytes revealed a non-autonomous role for Hippo signaling in those cells. Hippo-Yap signaling has been documented as regulating Notch signaling in the context of hepatocyte and biliary cell differentiation (Wu et al., 2017; Yimlamai et al., 2014). Notch signaling is also recognized as crucial for regulating proper intrahepatic biliary cell fate (Ko et al., 2019; Lorent et al., 2004, 2010; Russell et al., 2019). Of particular relevance, Wnt activity from hepatocytes has been shown to drive Notch activity in zebrafish biliary cells (So et al., 2018). Thus, the interactions of Hippo-Wnt-Notch signaling warrant further investigation for mediating the communication between hepatocytes and adjacent biliary epithelial cells.

Hippo signaling in the extrahepatic biliary system

Our experiments also addressed Hippo-Yap and Taz signaling in the extrahepatic biliary ducts. We found that either *sav1* or *stk3* deletion disrupted gallbladder and extrahepatic biliary network development and maintenance. Results in larvae showing rescue of these defects by *lfabp:*eGFP-2a:Sav1 expression in *sav1*$^{-/-}$ larvae argue that the

Development (2020) 147, dev184242. doi:10.1242/dev.184242

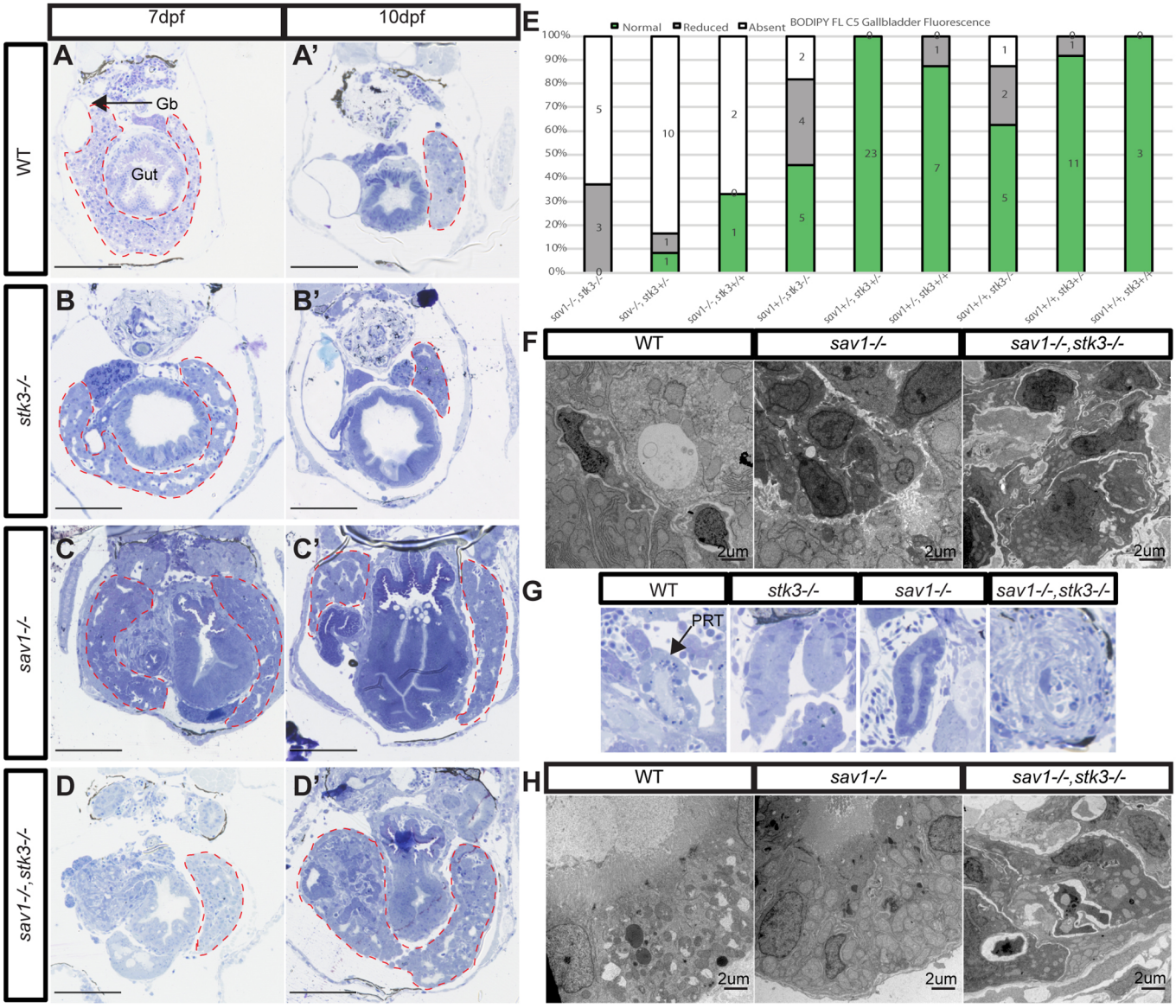

Fig. 11. *sav1* and *stk3* display a synergistic genetic interaction. (A-D′) Toluidine Blue stained Epon sections of liver and gallbladder in wild-type, *sav1*$^{-/-}$, *stk3*$^{-/-}$ and *sav1*$^{-/-}$;*stk3*$^{-/-}$ larvae at 7 and 10 dpf. Gb, gallbladder. Red dashed lines outline the liver. Scale bars: 100 µm. (E) Ratiometric analysis at 8 dpf of BODIPY FL C5 gallbladder uptake in larvae from a *sav1*$^{+/-}$;*stk3*$^{+/-}$ incross. (F) TEM of wild-type, *sav1*$^{-/-}$ and *sav1*$^{-/-}$;*stk3*$^{-/-}$ Epon sections at 10 dpf reveals the most severe phenotype in *sav1*$^{-/-}$;*stk3*$^{-/-}$ larvae. (G) Toluidine Blue stained epon sections of proximal renal tubules in wild-type, *sav1*$^{-/-}$, *stk3*$^{-/-}$ and *sav1*$^{-/-}$;*stk3*$^{-/-}$ larvae at 10 dpf. PRT, proximal renal tubule. Only double mutants display a dysplastic and fibrotic phenotype. (H) TEM of larvae from G.

phenotypes observed might be secondary to loss of Hippo signaling in hepatocytes. However, as *sav1*$^{-/-}$*; lfabp:*eGFP-2a:Sav1 mutants grow into adulthood, they lose distinguishable gallbladders and exhibit tissue masses resembling cholangiocarcinoma. This suggests that Sav1 expression in non-hepatocytes is also required for proper gallbladder maintenance. One hypothesis is that cells of the gallbladder and extrahepatic duct represent this non-hepatocyte population. An alternative hypothesis is that loss of Sav1 in hepatic stellate cells leads to the extrahepatic defects. In support of this possibility, *ctgfa:d2GFP*$^{+}$ cells, which resemble hepatic stellate cells, are increased in number and in Yap activity levels in *sav1*$^{-/-}$ mutants. Further work is required to identify the mechanisms leading to this adult phenotype. Evidence implicating the dysregulation of Yap in cholangiocarcinoma has accumulated recently, through analysis of both animal models and human tumor samples (Manmadhan and Ehmer, 2019; Sugihara et al., 2019; Werneburg et al., 2019). However these Hippo-associated cholangiocarcinoma animal models are exclusively intrahepatic in origin. These findings suggest *sav1*$^{-/-}$*; lfabp:*eGFP-2a:Sav1 fish may model cholangiocarcinoma, particularly those of extrahepatic origin. Together, our data argue that non-autonomous Hippo signaling is crucial for proper development of the gallbladder and extrahepatic ducts, and suggest a possible cell-autonomous role for Hippo signaling in their maintenance.

Hippo kinase redundancy

Both mice and humans contain *STK4* and *STK3* genes encoding MST1 and MST2 kinase, respectively. However, zebrafish contain only the *stk3* gene and no known ortholog of *STK4*. Given the temporal differences in phenotype manifestation between *sav1*$^{-/-}$ and *stk3*$^{-/-}$ larvae, we hypothesized that an unidentified kinase may function redundantly with Stk3 in this context. If Sav1 functions to

Development (2020) 147, dev184242. doi:10.1242/dev.184242

regulate Stk3 as well as a redundant kinase, *sav1*$^{-/-}$ mutants would effectively stop function of both kinases, explaining the earlier phenotypic onset. As PP2A inhibition reduced *ctgfa:*d2GFP expression back to wild-type levels in *sav1*$^{-/-}$ livers, we suggest that Sav1 regulates another kinase through this same mechanism. Indeed, there is recent evidence for kinases not canonically associated with Hippo signaling that impact Lats1/2 activation to regulate Yap. Several MAP4K family members were identified as regulators of Yap and Taz through direct phosphorylation of Lats1/2 (Meng et al., 2015). Sav1 interaction was investigated, but not found to associate with MAP4Ks. Similarly, an RNAi screen in IMR90 fibroblasts identified Stk25 as an upstream regulator of Yap through Lats1/2 activation; a role for Sav1 in this activation was not investigated (Lim et al., 2019). Tyrosine phosphorylation of Yap by the Src family kinase LCK has also recently been implicated in regulating Yap subcellular localization and transcriptional activity in the context of cholangiocarcinoma. Although these effects were independent of Lats1, a role for Sav1 in this context is unknown (Sugihara et al., 2018). In *Drosophila*, Sav1 and Hippo have been shown to use unique SARAH domains to interact (Cairns et al., 2018). Although Stk3 and Stk4 are the only identified Hippo pathway kinases containing a SARAH domain, our results suggest that Sav1 may regulate another kinase also regulated by PP2A.

Genetic interactions between Sav1 and Stk3

The sole function of Sav1 has currently been described to enhance activation of Stk3 and Stk4. With this in mind, we expected *sav1*$^{-/-}$; *stk3*$^{-/-}$ double mutants to phenocopy *sav1*$^{-/-}$ larvae. Surprisingly, we found double mutants showed more severe biliary phenotypes, with novel consequences to proximal kidney tubule morphology not observed in single *sav1*$^{-/-}$ or *stk3*$^{-/-}$ mutants. These results strongly suggest that Sav1 has functions other than enhancing Stk3 kinase activity. In support of this hypothesis, two separate research teams have found that conditional knockout of *sav1* in mice did not affect levels of phospho-Lats1/2 or phospho-Yap. Moreover, Yap was found to be enriched in the nucleus and Yap target genes were upregulated. These data are consistent with increased Yap activity, despite unaltered phosphorylation (Lee et al., 2010; Lu et al., 2010). Cumulatively, these observations suggest Sav1 can regulate Yap activity through mechanisms other than Hippo kinase activation and subsequent Yap phosphorylation.

In summary, our study reveals a vital role for *sav1* in zebrafish development, as *sav1*$^{-/-}$ mutants are unable to survive past larval stages. Analysis specifically uncovered a role for Hippo signaling in the extrahepatic biliary system, but also demonstrated the phylogenetic conservation of Hippo signaling in intrahepatic biliary ducts. We also present findings with important implications for the molecular mechanisms of Hippo signaling in this context. Results presented support a role for the phosphatase PP2A in liver development and define a synergistic genetic interaction in *sav1*$^{-/-}$; *stk3*$^{-/-}$ double mutants, suggesting Sav1 functions beyond augmenting Hippo kinase activity.

MATERIALS AND METHODS

Gateway cloning

The *sav1:eGFP-2a:sav1* plasmid and transgene were generated using Gateway (Invitrogen) entry clones and recombination with the Tol2 Kit (Kwan et al., 2007). RT-PCR was performed to generate a 3′ entry clone, including the full-length cDNA for *sav1* (Accession Number NM_001004560) with Gateway attB recombination sites attached at the 5′ end using the following primers: Sav1 attB2 FPrimer, 5′-GGGGACAGCTTTCTTGTACAAAGTGGCGGCCATGCTCTCCAGAAAGAAGAGT-3′; Sav1 attB3 RPrimer, 5′-GGGGACAGCTTTCTTGTACAAAGTGGCGGCCATGCTCTCCAGAAAGAAGAGT-3′.

The final 3′ entry clone was verified via sequencing (Retrogen), recombined with the previously generated −2.8 kb lfabp 5′ entry clone (Her et al., 2003) and eGFP-2a middle entry clone into the Tol2 plasmid, and injected into one- to four-cell embryos with transposase RNA. Embryos were screened for GFP expression in the liver, raised to adulthood and outcrossed to identify germline transmission of single copy transgenes.

Zebrafish

All transgenic and mutant lines were generated and maintained in the ZDR genetic background. Wild-type siblings of each line were used as control groups. All animal experiments were approved by the Institutional Animal Care and Use Committee of the Medical College of Wisconsin.

Transgenic lines

Tg(lfabp:eGFP-2a:sav1) was generated in this study. *Tg(ctgfa:d2GFP)* has been previously described (Miesfeld et al., 2015).

Mutant lines

Zebrafish mutant lines were generated in the ZDR genetic background by the following methods. Transcription activator-like effector nucleases (TALEN) designed against *stk3* were generated by Cellectis Bioresearch and supplied as plasmids. The left *stk3* TALEN arm targeted exon 2 (5′-TCAGTGAAGA-CAGTCTTACC-3′) and 15 nucleotides downstream in exon 2 was the right stk3 TALEN arm target sequence (5′-GTATTTGATGTTCTTGAAAAA-3′).

mRNA was generated from the supplied plasmids using the mMESSAGE mMACHINE, polyadenylated using the Poly(A) Tailing Kit (Ambion) and injected into one- to four-cell stage embryos at 150 pg per TALEN arm. Offspring from the *stk3* TALEN-injected embryos were screened using restriction sites within each spacer region, to identify founders.

Clustered regularly interspaced short palindromic repeats (CRISPRs) were designed against regions of zebrafish *sav1* exon2 using ZiFiT Targeter Version 4.2 (http://zifit.partners.org/ZiFiT, in the public domain). The targeted sequence was 5′-GGATCTGTTGGAGATGTTAG-3′. CRISPR gRNA templates were generated by cloning annealed oligonucleotides with appropriate overhangs into BsaI-digested pDR274 plasmid. CRISPR gRNAs were synthesized using the MEGAshortscript T7 Transcription Kit and purified using the mirVana miRNA Isolation Kit (Ambion). Zebrafish codon-optimized *cas9* was synthesized using the mMESSAGE mMACHINE Kit (Ambion) and polyadenylated using the Poly(A) Tailing Kit (Ambion). CRISPR gRNAs and *cas9* mRNA were injected into one- to four-cell zebrafish embryos at 12.5 ng/µl and 300 ng/µl, respectively, and surviving embryos raised to adulthood before outcrossing to identify founder fish carrying germline edits in *sav1*. Offspring from these fish were raised to adulthood, then fin-clipped for genotyping (see below for details). The resulting 11 bp insertion mutant described here was identified via sequencing (Retrogen).

Plastic histology and TEM

Larvae were fixed with 1.0% paraformaldehyde, 2.5% glutaraldehyde and 3.0% sucrose in 0.06 M phosphate buffer overnight at 4°C. Samples were then washed three times in phosphate buffer, post-fixed with 1% osmium tetroxide and dehydrated by a series of methanol washes. Larvae were infused with Epon 812 resin (Electron Microscopy Sciences) through two 15 min acetonitrile washes followed by 1:1 acetonitrile:Epon incubation for 1 h and 100% Epon incubation overnight. Finally, larvae were embedded in 100% Epon and hardened at 65°C for 24 h. 1 µm transverse serial sections through the length of the larvae were cut using a microtome and stained with Toluidine Blue for light microscopy. Light microscopy images were taken using a NanoZoomer 2.0-HT (Hamamatsu Photonics). For TEM analysis 70 nm sections were cut, collected on hexagonal grids and stained with uranyl acetate and lead citrate, followed by imaging on a Hitachi H-600 electron microscope.

Paraffin histology

Larvae used for paraffin histology were immersed in 4% paraformaldehyde overnight at 4°C and embedded in paraffin blocks for sectioning. Sections (4 µm) were obtained and stained with Hematoxylin and Eosin for analysis,

Development (2020) 147, dev184242. doi:10.1242/dev.184242

with serial unstained sections used for immunofluorescent staining. Unstained sections underwent de-paraffinization with xylenes and an ethanol gradient prior to heated antigen retrieval in antigen retrieval solution (Dako). Immunofluorescent staining was then performed as follows.

Immunofluorescence

Whole-mount immunohistochemistry was performed on larvae or dissected tissues that were fixed overnight at 4°C in 4% paraformaldehyde. Before whole-mount staining, the skin of larvae was dissected away to allow better access to the tissue of interest. Larvae were washed in PBS to remove fixative and taken through a methanol dehydration series to 100% methanol. To increase permeabilization, larvae were rehydrated and washed with acetone before incubating in 100% acetone for at least 1 h. Standard immunostaining followed with a 1 h incubation in blocking solution (2% normal goat serum, 1% TritonX-100 and 1% Tween-20 in PBS). Larvae were incubated in primary antibodies overnight in blocking solution at room temperature or 4°C. Embryos were then washed three times for 1 h in 1% Tween-20 in PBS. Antibody detection was performed using AlexaFluor(488, 568, and 633) conjugated secondary antibodies from Invitrogen at 1:800 dilution in blocking solution overnight at 4°C followed by washes with 1% Tween-20 in PBS. The following primary antibodies and concentrations were used: 1:200 dilution rabbit monoclonal Yap (ab81183, Abcam), 1:200 dilution rabbit monoclonal Yap and Taz (D24E4, Cell Signaling, 8418), 1:500 dilution rabbit monoclonal GFP (G10362, ABfinity), 1:100 dilution mouse polyclonal Alcam (zn-8, DSHB), 1:200 dilution mouse monoclonal AnnexinA4/2F11 [ab71286, Zebrafish Gut Secretory Cell Epitope (FIS2F11/2)], 1:500 dilution rabbit polyclonal aPKC λ and ξ (C-20 and sc-216, Santa Cruz Biotech), 1:200 dilution rabbit polyclonal Cdh2 (GTX125962, GeneTex) and 1:500 dilution rabbit polyclonal Prox1 (AB5475, EMD Millipore).

Fluorescent microscopy

Zebrafish embryos were raised in 0.003% N-phenylthiourea (PTU, Sigma Aldrich) and examined for transgenic expression eGFP or d2GFP constructs using a Leica MZFLIII fluorescent dissection microscope. Confocal microscopy was performed using a Nikon Eclipse E800 confocal microscope on larvae anesthetized in 3-amino benzoic acid ethyl ester (Tricaine, Sigma Aldrich) and embedded in 1% low-melting agarose in glass-bottomed Petri dishes. Images were generated using the Nikon EZ-C1 viewer (Nikon Instruments) and ImageJ (NIH) software.

BODIPY C5 FL fluorescence

8 dpf larvae were bathed in 10 µM green fluorescent fatty acid BODIPY FL C5 (4,4-Difluoro-5,7-Dimethyl-4-Bora-3a,4a-Diaza-s-Indacene-3-Pentanoic Acid, ThermoFisher) for 1 h prior to analysis. Larvae were then anesthetized in tricaine, rinsed briefly in fish water and gallbladders were scored blindly as having bright, dim or no fluorescence (no fluorescence included embryos with no identifiable gallbladder). Fluorescence was visualized using a Leica MZFLIII fluorescent dissection microscope.

LB100 treatment

Larvae from a *sav1*+/−*;ctgfa:d2GFP* in-cross were bathed in 20 µM LB100 and 0.02% PBS in fish water continuously, with the water being switched out every 48 h from 4.5 dpf to 7.5 dpf. Vehicle control siblings were treated with 0.02% PBS in fish water simultaneously. All larvae were imaged and analyzed for fluorescent intensity blindly, prior to genotyping. Fluorescent intensity was assessed using ImageJ software.

EdU incorporation assay

To assess DNA synthesis, larvae were bathed in 70 µM 5-ethynyl-2′-deoxyuridine (EdU), 0.003% PTU and 0.176% dimethyl sulfoxide (DMSO) in fish water for 24 h from 7.5 dpf to 8.5 dpf. EdU incorporation was detected using the Click-iT EdU Assay kit (Invitrogen). EdU^+ gallbladder cells were counted for statistical analysis using ImageJ software.

Western blotting

Wild-type and $stk3^{-/-}$ whole embryos were processed in lysis buffer and centrifuged as previously described. The supernatants were boiled for 5 min in SDS sample buffer, fractionated by SDS-PAGE (7.5% Mini-Protean TGX, Bio-Rad), with one lane corresponding to one whole-embryo lysate, and transferred to Immobilon FL PVDF membranes (Millipore). Membranes were incubated for 1 h at room temperature in Odyssey blocking buffer (LI-COR Biosciences), and incubated overnight at 4°C with primary antibodies diluted in Odyssey blocking buffer, then with near infrared fluorescent secondary antibodies (IRDye 680RD and IRDye 800CW, LI-COR Biosciences) for 1 h at room temperature. Proteins were detected with an Odyssey infrared imager (LI-COR Biosciences). Stk3 was detected using a 1:1000 dilution of rabbit α-Stk3 (Abcam, ab70546), and γ-tubulin with a 1:200 dilution of mouse α-γ-tubulin (Sigma, T6557).

Genotyping

Genomic DNA was extracted from zebrafish tissue using the Puregene Core Kit (Qiagen). The genomic region containing the mutation of interest was amplified by PCR, and examined for the gain or loss of a restriction site. The *sav1* 11 bp insertion was detected by loss of a NlaIII or BslI restriction site. The *stk3* 5 bp deletion was detected by loss of a MnlI restriction site.

Acknowledgements

Our appreciation extends to the Children's Research Institute Histology Core for assistance with routine histology and immunohistochemistry, to Clive Wells for assistance with transmission electron microscopy, and to all members of the Link Lab for constructive criticism.

Competing interests

The authors declare no competing or financial interests.

Author contributions

Conceptualization: Z.J.B., B.A.L.; Methodology: Z.J.B., A.E.E., J.R.B.; Formal analysis: Z.J.B., P.N.N., B.A.L.; Investigation: Z.J.B., A.E.E., J.R.B., P.N.N., B.A.L.; Writing - original draft: Z.J.B.; Writing - review & editing: Z.J.B., P.N.N., B.A.L.; Supervision: B.A.L.; Project administration: B.A.L.; Funding acquisition: B.A.L.

Funding

This work was supported by the National Institutes of Health/National Eye Institute (R01EY029267 to B.A.L.) and funds provided by the Cancer Center of the Medical College of Wisconsin. Deposited in PMC for release after 12 months.

Supplementary information

Supplementary information available online at
http://dev.biologists.org/lookup/doi/10.1242/dev.184242.supplemental

Peer review history

The peer review history is available online at
https://dev.biologists.org/lookup/doi/10.1242/dev.184242.reviewer-comments.pdf

References

Bae, S. J., Ni, L., Osinski, A., Tomchick, D. R., Brautigam, C. A. and Luo, X. (2017). SAV1 promotes Hippo kinase activation through antagonizing the PP2A phosphatase STRIPAK. *eLife* **6**, e30278. doi:10.7554/eLife.30278

Benhamouche, S., Curto, M., Saotome, I., Gladden, A. B., Liu, C.-H., Giovannini, M. and McClatchey, A. I. (2010). Nf2/Merlin controls progenitor homeostasis and tumorigenesis in the liver. *Genes Dev.* **24**, 1718-1730. doi:10.1101/gad.1938710

Cairns, L., Tran, T., Fowl, B. H., Patterson, A., Kim, Y. J., Bothner, B. and Kavran, J. M. (2018). Salvador has an extended SARAH domain that mediates binding to Hippo kinase. *J. Biol. Chem.* **293**, 5532-5543. doi:10.1074/jbc.RA117.000923

Camargo, F. D., Gokhale, S., Johnnidis, J. B., Fu, D., Bell, G. W., Jaenisch, R. and Brummelkamp, T. R. (2007). YAP1 increases organ size and expands undifferentiated progenitor cells. *Curr. Biol.* **17**, 2054-2060. doi:10.1016/j.cub.2007.10.039

Cerami, E., Gao, J., Dogrusoz, U., Gross, B. E., Sumer, S. O., Aksoy, B. A., Jacobsen, A., Byrne, C. J., Heuer, M. L., Larsson, E. et al. (2012). The cBio cancer genomics portal: an open platform for exploring multidimensional cancer genomics data. *Cancer Discov.* **2**, 401-404. doi:10.1158/2159-8290.CD-12-0095

Cofer, Z. C., Cui, S., EauClaire, S. F., Kim, C., Tobias, J. W., Hakonarson, H., Loomes, K. M. and Matthews, R. P. (2016). Methylation microarray studies highlight PDGFA expression as a factor in biliary atresia. *PLoS ONE* **11**, e0151521. doi:10.1371/journal.pone.0151521

Cox, A. G., Hwang, K. L., Brown, K. K., Evason, K. J., Beltz, S., Tsomides, A., O'Connor, K., Galli, G. G., Yimlamai, D., Chhangawala, S. et al. (2016). Yap

reprograms glutamine metabolism to increase nucleotide biosynthesis and enable liver growth. *Nat. Cell Biol.* **18**, 886-896. doi:10.1038/ncb3389

Cox, A. G., Tsomides, A., Yimlamai, D., Hwang, K. L., Miesfeld, J., Galli, G. G., Fowl, B. H., Fort, M., Ma, K. Y., Sullivan, M. R. et al. (2018). Yap regulates glucose utilization and sustains nucleotide synthesis to enable organ growth. *EMBO J.* **37**, e100294. doi:10.15252/embj.2018100294

Delous, M., Yin, C., Shin, D., Ninov, N., Carten, J. D., Pan, L., Ma, T. P., Farber, S. A., Moens, C. B. and Stainier, D. Y. R. (2012). sox9b is a key regulator of pancreaticobiliary ductal system development. *PLoS Genet.* **8**, e1002754. doi:10.1371/journal.pgen.1002754

Deutschmann, K., Reich, M., Klindt, C., Dröge, C., Spomer, L., Häussinger, D. and Keitel, V. (2018). Bile acid receptors in the biliary tree: TGR5 in physiology and disease. *Biochim. Biophys. Acta Mol. Basis Dis.* **1864**, 1319-1325. doi:10.1016/j.bbadis.2017.08.021

Dong, P. D. S., Munson, C. A., Norton, W., Crosnier, C., Pan, X., Gong, Z., Neumann, C. J. and Stainier, D. Y. R. (2007). Fgf10 regulates hepatopancreatic ductal system patterning and differentiation. *Nat. Genet.* **39**, 397-402. doi:10.1038/ng1961

Ellis, J. L., Bove, K. E., Schuetz, E. G., Leino, D., Valencia, C. A., Schuetz, J. D., Miethke, A. and Yin, C. (2018). Zebrafish abcb11b mutant reveals strategies to restore bile excretion impaired by bile salt export pump deficiency. *Hepatology* **67**, 1531-1545. doi:10.1002/hep.29632

Gao, J., Aksoy, B. A., Dogrusoz, U., Dresdner, G., Gross, B., Sumer, S. O., Sun, Y., Jacobsen, A., Sinha, R., Larsson, E. et al. (2013). Integrative analysis of complex cancer genomics and clinical profiles using the cBioPortal. *Sci. Signal* **6**, pl1. doi:10.1126/scisignal.6273er1

Gao, C., Huang, W., Gao, Y., Lo, L. J., Luo, L., Huang, H., Chen, J. and Peng, J. (2019). Zebrafish hhex-null mutant develops an intrahepatic intestinal tube due to de-repression of cdx1b and pdx1. *J. Mol. Cell Biol.* **11**, 448-462. doi:10.1093/jmcb/mjy068

Hamaratoglu, F., Willecke, M., Kango-Singh, M., Nolo, R., Hyun, E., Tao, C., Jafar-Nejad, H. and Halder, G. (2006). The tumour-suppressor genes NF2/Merlin and Expanded act through Hippo signalling to regulate cell proliferation and apoptosis. *Nat. Cell Biol.* **8**, 27-36. doi:10.1038/ncb1339

Her, G. M., Chiang, C.-C., Chen, W.-Y. and Wu, J.-L. (2003). In vivo studies of liver-type fatty acid binding protein (L-FABP) gene expression in liver of transgenic zebrafish (Danio rerio). *FEBS Lett.* **538**, 125-133. doi:10.1016/S0014-5793(03)00157-1

Hong, C. S., Ho, W., Zhang, C., Yang, C., Elder, J. B. and Zhuang, Z. (2015). LB100, a small molecule inhibitor of PP2A with potent chemo- and radio-sensitizing potential. *Cancer Biol. Ther.* **16**, 821-833. doi:10.1080/15384047.2015.1040961

Keplinger, K. M. and Bloomston, M. (2014). Anatomy and embryology of the biliary tract. *Surgical Clinics of North America* **94**, 203-217. doi:10.1016/j.suc.2014.01.001

Kimelman, D., Smith, N. L., Lai, J. K. H. and Stainier, D. Y. R. (2017). Regulation of posterior body and epidermal morphogenesis in zebrafish by localized Yap1 and Wwtr1. *eLife* **6**, e31065. doi:10.7554/eLife.31065

Ko, S., Russell, J. O., Tian, J., Gao, C., Kobayashi, M., Feng, R., Yuan, X., Shao, C., Ding, H., Poddar, M. et al. (2019). Hdac1 regulates differentiation of bipotent liver progenitor cells during regeneration via Sox9b and Cdk8. *Gastroenterology* **156**, 187-202.e14. doi:10.1053/j.gastro.2018.09.039

Kwan, K. M., Fujimoto, E., Grabher, C., Mangum, B. D., Hardy, M. E., Campbell, D. S., Parant, J. M., Yost, H. J., Kanki, J. P. and Chien, C.-B. (2007). The Tol2kit: a multisite gateway-based construction kit for Tol2 transposon transgenesis constructs. *Dev. Dyn.* **236**, 3088-3099. doi:10.1002/dvdy.21343

Lai, J. K. H., Collins, M. M., Uribe, V., Jiménez-Amilburu, V., Günther, S., Maischein, H.-M. and Stainier, D. Y. R. (2018). The Hippo pathway effector Wwtr1 regulates cardiac wall maturation in zebrafish. *Development* **145**, dev159210. doi:10.1242/dev.159210

Lee, J.-H., Kim, T.-S., Yang, T.-H., Koo, B.-K., Oh, S.-P., Lee, K.-P., Oh, H.-J., Lee, S.-H., Kong, Y.-Y., Kim, J.-M. et al. (2008). A crucial role of WW45 in developing epithelial tissues in the mouse. *EMBO J.* **27**, 1231-1242. doi:10.1038/emboj.2008.63

Lee, K.-P., Lee, J.-H., Kim, T.-S., Kim, T.-H., Park, H.-D., Byun, J.-S., Kim, M.-C., Jeong, W.-I., Calvisi, D. F., Kim, J.-M. et al. (2010). The Hippo–Salvador pathway restrains hepatic oval cell proliferation, liver size, and liver tumorigenesis. *Proc. Natl. Acad. Sci. USA* **107**, 8248-8253. doi:10.1073/pnas.0912203107

Lee, D.-H., Park, J. O., Kim, T.-S., Kim, S.-K., Kim, T.-H., Kim, M.-C., Park, G. S., Kim, J.-H., Kuninaka, S., Olson, E. N. et al. (2016). LATS-YAP/TAZ controls lineage specification by regulating TGFβ signaling and Hnf4α expression during liver development. *Nat. Commun.* **7**, 11961. doi:10.1038/ncomms11961

Lemaigre, F. P. (2019). Development of the Intrahepatic and Extrahepatic Biliary Tract: A Framework for Understanding Congenital Diseases. *Httpsdoiorg101146annurev-Pathmechdis*-012418-013013.

Lim, S., Hermance, N., Mudianto, T., Mustaly, H. M., Mauricio, I. P. M., Vittoria, M. A., Quinton, R. J., Howell, B. W., Cornils, H., Manning, A. L. et al. (2019). Identification of the kinase STK25 as an upstream activator of LATS signaling. *Nat. Commun.* **10**, 1547. doi:10.1038/s41467-019-09597-w

Lorent, K., Yeo, S.-Y., Oda, T., Chandrasekharappa, S., Chitnis, A., Matthews, R. P. and Pack, M. (2004). Inhibition of Jagged-mediated Notch signaling disrupts zebrafish biliary development and generates multi-organ defects compatible with an Alagille syndrome phenocopy. *Development* **131**, 5753-5766. doi:10.1242/dev.01411

Lorent, K., Moore, J. C., Siekmann, A. F., Lawson, N. and Pack, M. (2010). Reiterative use of the notch signal during zebrafish intrahepatic biliary development. *Dev. Dyn.* **239**, 855-864. doi:10.1002/dvdy.22220

Lorent, K., Gong, W., Koo, K. A., Waisbourd-Zinman, O., Karjoo, S., Zhao, X., Sealy, I., Kettleborough, R. N., Stemple, D. L., Windsor, P. A. et al. (2015). Identification of a plant isoflavonoid that causes biliary atresia. *Sci. Transl. Med.* **7**, 286ra67. doi:10.1126/scitranslmed.aaa1652

Lu, J., Kovach, J. S., Johnson, F., Chiang, J., Hodes, R., Lonser, R. and Zhuang, Z. (2009). Inhibition of serine/threonine phosphatase PP2A enhances cancer chemotherapy by blocking DNA damage induced defense mechanisms. *Proc. Natl. Acad. Sci. USA* **106**, 11697-11702. doi:10.1073/pnas.0905930106

Lu, L., Li, Y., Kim, S. M., Bossuyt, W., Liu, P., Qiu, Q., Wang, Y., Halder, G., Finegold, M. J., Lee, J.-S. et al. (2010). Hippo signaling is a potent in vivo growth and tumor suppressor pathway in the mammalian liver. *Proc. Natl. Acad. Sci. USA* **107**, 1437-1442. doi:10.1073/pnas.0911427107

Manfroid, I., Ghaye, A., Naye, F., Detry, N., Palm, S., Pan, L., Ma, T. P., Huang, W., Rovira, M., Martial, J. A. et al. (2012). Zebrafish sox9b is crucial for hepatopancreatic duct development and pancreatic endocrine cell regeneration. *Dev. Biol.* **366**, 268-278. doi:10.1016/j.ydbio.2012.04.002

Manmadhan, S. and Ehmer, U. (2019). Hippo signaling in the liver – a long and ever-expanding story. *Front. Cell Dev. Biol.* **7**, 33. doi:10.3389/fcell.2019.00033

Martinot, E., Sèdes, L., Baptissart, M., Lobaccaro, J.-M., Caira, F., Beaudoin, C. and Volle, D. H. (2017). Bile acids and their receptors. *Mol. Aspects Med.* **56**, 2-9. doi:10.1016/j.mam.2017.01.006

McClatchey, A. I., Saotome, I., Mercer, K., Crowley, D., Gusella, J. F., Bronson, R. T. and Jacks, T. (1998). Mice heterozygous for a mutation at the Nf2 tumor suppressor locus develop a range of highly metastatic tumors. *Genes Dev.* **12**, 1121-1133. doi:10.1101/gad.12.8.1121

McPherson, J. P., Tamblyn, L., Elia, A., Migon, E., Shehabeldin, A., Matysiak-Zablocki, E., Lemmers, B., Salmena, L., Hakem, A., Fish, J. et al. (2004). Lats2/Kpm is required for embryonic development, proliferation control and genomic integrity. *EMBO J.* **23**, 3677-3688. doi:10.1038/sj.emboj.7600371

Meng, Z., Moroishi, T., Mottier-Pavie, V., Plouffe, S. W., Hansen, C. G., Hong, A. W., Park, H. W., Mo, J.-S., Lu, W., Lu, S. et al. (2015). MAP4K family kinases act in parallel to MST1/2 to activate LATS1/2 in the Hippo pathway. *Nat. Commun.* **6**, 8357. doi:10.1038/ncomms9357

Meyer, K., Morales-Navarrete, H., Seifert, S., Wilsch-Braeuninger, M., Dahmen, U., Tanaka, E. M., Brusch, L., Kalaidzidis, Y. and Zerial, M. (2020). Bile canaliculi remodeling activates YAP via the actin cytoskeleton during liver regeneration. *Mol. Syst. Biol.* **16**, e8985. doi:10.15252/msb.20198985

Miesfeld, J. B., Gestri, G., Clark, B. S., Flinn, M. A., Poole, R. J., Bader, J. R., Besharse, J. C., Wilson, S. W. and Link, B. A. (2015). Yap and Taz regulate retinal pigment epithelial cell fate. *Development* **142**, 3021-3032. doi:10.1242/dev.119008

Nishio, M., Sugimachi, K., Goto, H., Wang, J., Morikawa, T., Miyachi, Y., Takano, Y., Hikasa, H., Itoh, T., Suzuki, S. O. et al. (2016). Dysregulated YAP1/TAZ and TGF-β signaling mediate hepatocarcinogenesis in Mob1a/1b-deficient mice. *Proc. Natl. Acad. Sci. USA* **113**, E71-E80. doi:10.1073/pnas.1517188113

Oh, S., Lee, D., Kim, T., Kim, T.-S., Oh, H. J., Hwang, C. Y., Kong, Y.-Y., Kwon, K.-S. and Lim, D.-S. (2009). Crucial role for Mst1 and Mst2 kinases in early embryonic development of the mouse. *Mol. Cell. Biol.* **29**, 6309-6320. doi:10.1128/MCB.00551-09

Pepe-Mooney, B. J., Dill, M. T., Alemany, A., Ordovas-Montanes, J., Matsushita, Y., Rao, A., Sen, A., Miyazaki, M., Anakk, S., Dawson, P. A. et al. (2019). Single-cell analysis of the liver epithelium reveals dynamic heterogeneity and an essential role for YAP in homeostasis and regeneration. *Cell Stem Cell* **25**, 23-38.e8. doi:10.1016/j.stem.2019.04.004

Pham, D.-H. and Yin, C. (2019). Zebrafish as a model to study cholestatic liver diseases. In *Experimental Cholestasis Research* (ed. M. Vinken), pp. 273-289. New York, NY: Springer New York.

Russell, J. O., Ko, S., Monga, S. P. and Shin, D. (2019). Notch inhibition promotes differentiation of liver progenitor cells into hepatocytes via sox9b repression in zebrafish. *Stem Cells Int.* **2019**, 8451282. doi:10.1155/2019/8451282

Sadler, K. C., Amsterdam, A., Soroka, C., Boyer, J. and Hopkins, N. (2005). A genetic screen in zebrafish identifies the mutants vps18, nf2 and foie gras as models of liver disease. *Development* **132**, 3561-3572. doi:10.1242/dev.01918

Sakaguchi, T. F., Sadler, K. C., Crosnier, C. and Stainier, D. Y. R. (2008). Endothelial signals modulate hepatocyte apicobasal polarization in zebrafish. *Curr. Biol.* **18**, 1565-1571. doi:10.1016/j.cub.2008.08.065

Shin, D., Lee, Y., Poss, K. D. and Stainier, D. Y. R. (2011). Restriction of hepatic competence by Fgf signaling. *Development* **138**, 1339-1348. doi:10.1242/dev.054395

So, J., Khaliq, M., Evason, K., Ninov, N., Martin, B. L., Stainier, D. Y. R. and Shin, D. (2018). Wnt/β-catenin signaling controls intrahepatic biliary network formation in zebrafish by regulating notch activity. *Hepatology* **67**, 2352-2366. doi:10.1002/hep.29752

Spence, J. R., Lange, A. W., Lin, S.-C. J., Kaestner, K. H., Lowy, A. M., Kim, I., Whitsett, J. A. and Wells, J. M. (2009). Sox17 regulates organ lineage segregation of ventral foregut progenitor cells. *Dev. Cell* **17**, 62-74. doi:10.1016/j.devcel.2009.05.012

Sugihara, T., Werneburg, N. W., Hernandez, M. C., Yang, L., Kabashima, A., Hirsova, P., Yohanathan, L., Sosa, C., Truty, M. J., Vasmatzis, G. et al. (2018). YAP tyrosine phosphorylation and nuclear localization in cholangiocarcinoma cells are regulated by LCK and independent of LATS activity. *Mol. Cancer Res.* **16**, 1556-1567. doi:10.1158/1541-7786.MCR-18-0158

Sugihara, T., Isomoto, H., Gores, G. and Smoot, R. (2019). YAP and the Hippo pathway in cholangiocarcinoma. *J. Gastroenterol.* **54**, 485-491. doi:10.1007/s00535-019-01563-z

Thestrup, M. I., Caviglia, S., Cayuso, J., Heyne, R. L. S., Ahmad, R., Hofmeister, W., Satriano, L., Wilkinson, D. G., Andersen, J. B. and Ober, E. A. (2019). A morphogenetic EphB/EphrinB code controls hepatopancreatic duct formation. *Nat. Commun.* **10**, 5220. doi:10.1038/s41467-019-13149-7

Villasenor, A. and Stainier, D. Y. R. (2017). On the development of the hepatopancreatic ductal system. *Semin. Cell Dev. Biol.* **66**, 69-80. doi:10.1016/j.semcdb.2017.02.003

Villasenor, A., Gauvrit, S., Collins, M. M., Maischein, H.-M. and Stainier, D. Y. R. (2020). Hhex regulates the specification and growth of the hepatopancreatic ductal system. *Dev. Biol.* **458**, 228-236. doi:10.1016/j.ydbio.2019.10.021

Werneburg, N., Gores, G. J. and Smoot, R. L. (2019). The hippo pathway and YAP signaling: emerging concepts in regulation, signaling, and experimental targeting strategies with implications for hepatobiliary malignancies. *Gene Expr.* doi:10.3727/105221619X15617324583639

Wilkins, B. J., Gong, W. and Pack, M. (2014). A novel keratin18 promoter that drives reporter gene expression in the intrahepatic and extrahepatic biliary system allows isolation of cell-type specific transcripts from zebrafish liver. *Gene Expr. Patterns* **14**, 62-68. doi:10.1016/j.gep.2013.12.002

Wu, N., Nguyen, Q., Wan, Y., Zhou, T., Venter, J., Frampton, G. A., DeMorrow, S., Pan, D., Meng, F., Glaser, S. et al. (2017). The Hippo signaling functions through the Notch signaling to regulate intrahepatic bile duct development in mammals. *Lab. Invest.* **97**, 843-853. doi:10.1038/labinvest.2017.29

Yi, J., Lu, L., Yanger, K., Wang, W., Sohn, B. H., Stanger, B. Z., Zhang, M., Martin, J. F., Ajani, J. A., Chen, J. et al. (2016). Large tumor suppressor homologs 1 and 2 regulate mouse liver progenitor cell proliferation and maturation through antagonism of the coactivators YAP and TAZ. *Hepatology* **64**, 1757-1772. doi:10.1002/hep.28768

Yimlamai, D., Christodoulou, C., Galli, G. G., Yanger, K., Pepe-Mooney, B., Gurung, B., Shrestha, K., Cahan, P., Stanger, B. Z. and Camargo, F. D. (2014). Hippo pathway activity influences liver cell fate. *Cell* **157**, 1324-1338. doi:10.1016/j.cell.2014.03.060

Zhang, N., Bai, H., David, K. K., Dong, J., Zheng, Y., Cai, J., Giovannini, M., Liu, P., Anders, R. A. and Pan, D. (2010). The Merlin/NF2 tumor suppressor functions through the YAP oncoprotein to regulate tissue homeostasis in mammals. *Dev. Cell* **19**, 27-38. doi:10.1016/j.devcel.2010.06.015

Zhang, D., Golubkov, V. S., Han, W., Correa, R. G., Zhou, Y., Lee, S., Strongin, A. Y. and Dong, P. D. S. (2014). Identification of Annexin A4 as a hepatopancreas factor involved in liver cell survival. *Dev. Biol.* **395**, 96-110. doi:10.1016/j.ydbio.2014.08.025

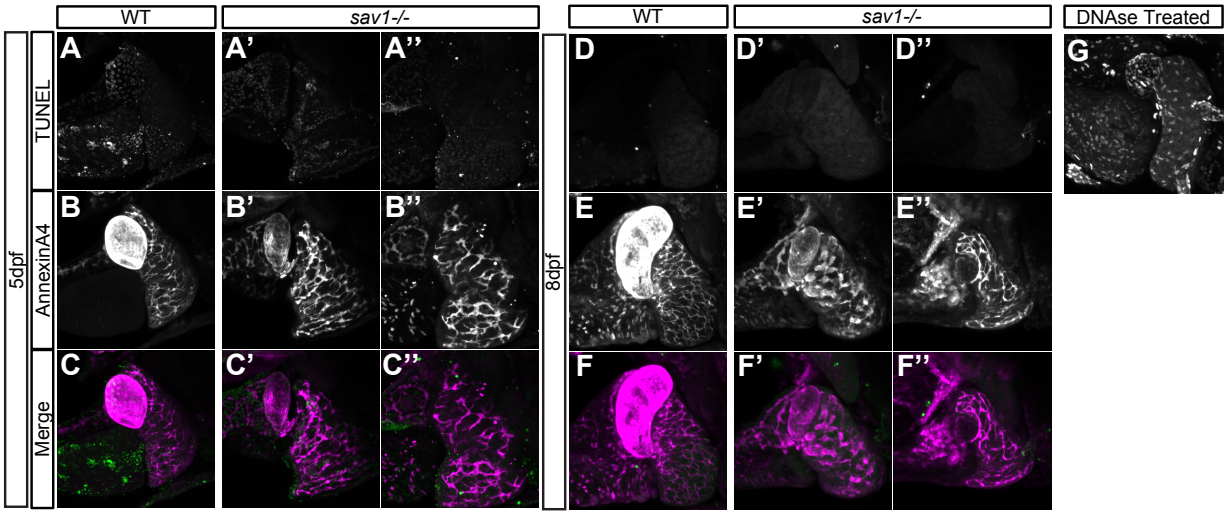

Figure S1. Abnormal biliary duct morphology, and loss of AnnexinA4 in gallbladder of *sav1-/-* larvae is not associated with biliary cell death. (A-A'') TUNEL staining of WT and *sav1-/-* larvae at 5dpf. There is no significant detection of TUNEL labeling at this time point in either WT or *sav1-/-* larvae regardless of phenotype severity. (B-B'') AnnexinA4 labeling in WT and *sav1-/-* fish to indicate phenotype severity. (C-C'') Merged images of A-A'' and B-B'' with AnnexinA4 stain in magenta, and TUNEL stain in green. *n=6* WT; *n=8 sav1-/-*. (D-F'') These panels depict TUNEL and AnnexinA4 whole-mount staining following the same labeling convention as A-C'' but at 8dpf. *n=4* WT; *n=11 sav1-/-*. (G) WT larvae at 8dpf treated with DNAse for 15 min serves as a positive control for TUNEL detection.

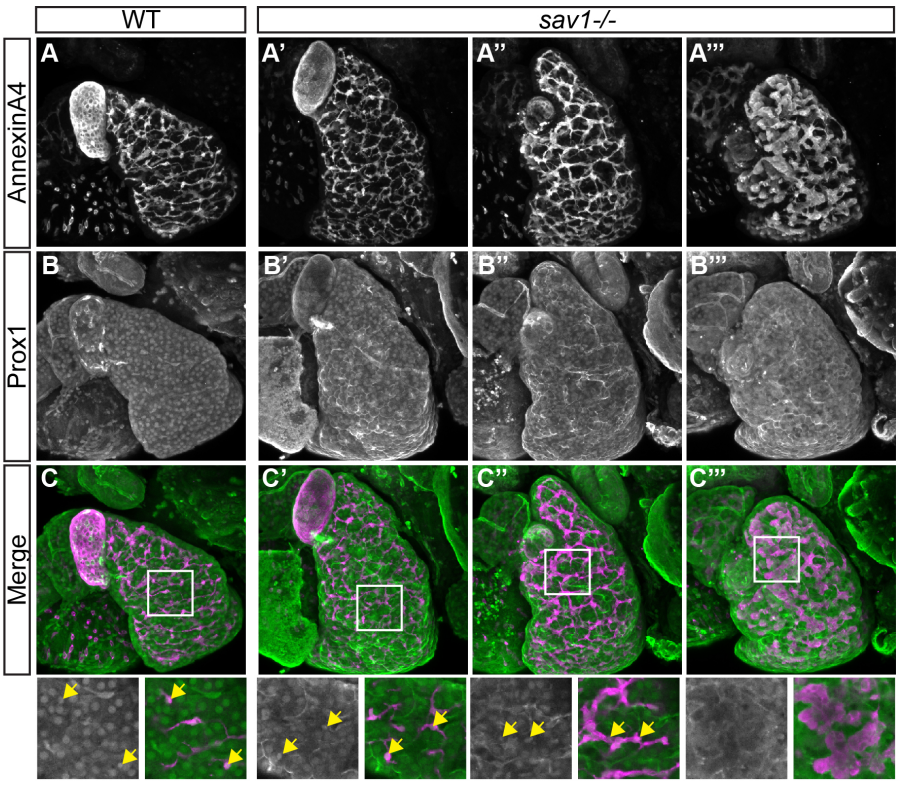

Figure S2. *sav1-/-* mutants lose Prox1 immunostaining in biliary cells with abnormal morphology. (A-A’’’) Whole-mount staining for AnnexinA4 in WT and *sav1-/-* larvae at 8dpf. (B-B’’’) Whole-mount staining of the same larvae from A-A’’’ for Prox1. (C-C’’’) Merged images of A-A’’’ and B-B’’’ with AnnexinA4 stain in magenta, and Prox1 stain in green. Single plane enlarged images corresponding to the white boxes shown in C-C’’’ are found below each merged image, with the left image showing grayscale Prox1 staining, and the right image depicting the merged image. Yellow arrows point to nuclear localized Prox1 labeling of intrahepatic biliary epithelial cells. Prox1 labels nuclei of both hepatocytes and biliary epithelial cells at 8dpf in WT and *sav1-/-* mutants characterized as normal or mild. Biliary epithelia in mutants with moderate or severe phenotypes lose Prox1 labeling. *n=4* WT; *n=7 sav1-/-*.

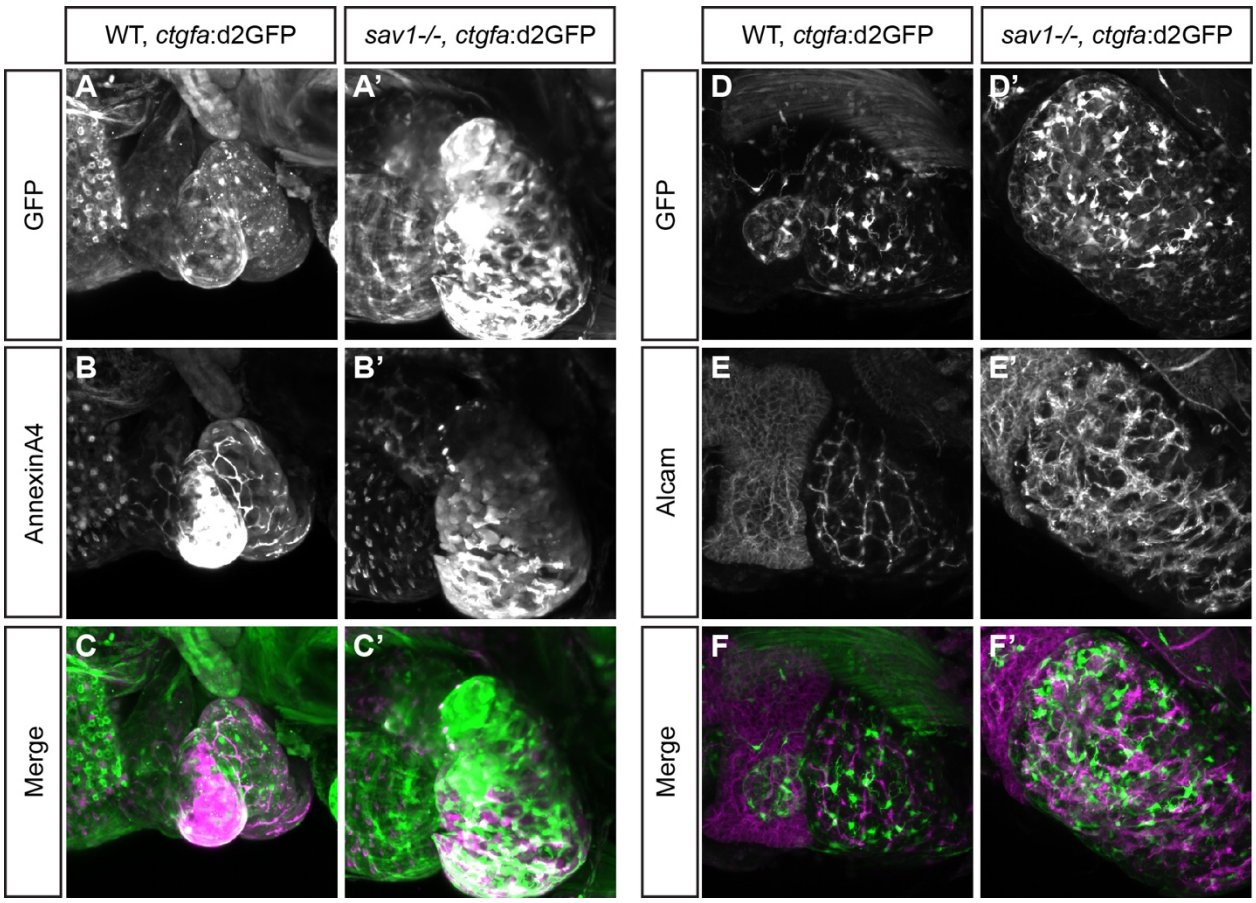

Figure S3. The Yap/Taz reporter *ctgfa*:d2GFP is elevated in both biliary cells and nonbiliary cells with deletion of *sav1*. (A-A', D-D') GFP staining of WT and *sav1-/-* larvae at 7dpf. WT fish show expression in gallbladder and sporadic cells located throughout the liver. (B-B') AnnexinA4 staining of WT and *sav1-/-* larvae at 8dpf. (C-C') Merged images of A-A' and B-B' with AnnexinA4 in magenta, and GFP in green. *n=5* WT; *n=4 sav1-/-*. Merged images show that in WT larvae *ctgfa*:d2GFP+ cells within the liver are often distinct from the intrahepatic biliary network with their morphology resembling hepatic stellate cells. In *sav1-/-* mutants, the fluorescent intensity and number of these cells are increased. *ctgfa*:d2GFP also is more highly expressed in *sav1-/-* mutant AnnexinA4+ cells with abnormal morphology. (E-E') Alcam staining of WT and *sav1-/-* larvae at 8dpf. (F-F') Merged images of A-A' and B-B' with AnnexinA4 in magenta, and GFP in green. *n=5,* WT; *n=6, sav1-/-*. Merged images show the majority of *ctgfa*:d2GFP+ cells in WT larvae are distinct from Alcam outlined biliary network.

Again in *sav1-/-* mutants, *ctgfa*:d2GFP expression is present in these nonbiliary cells as well as in Alcam+ cells with abnormal morphology.

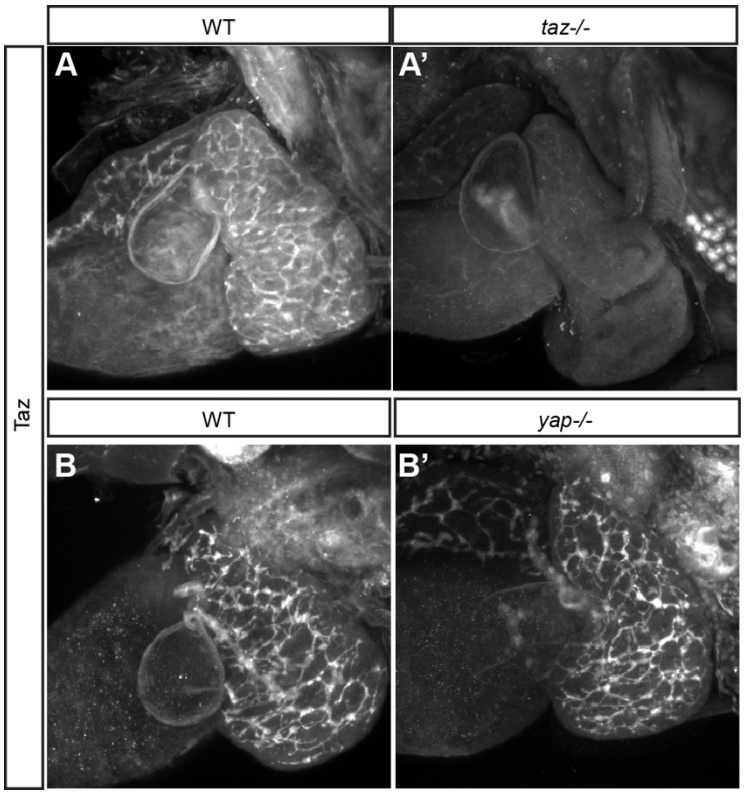

Figure S4. The Yap/Taz Cell Signaling antibody D24E4 selectively labels Taz within the biliary system. (A,B) Yap/Taz Cell signaling antibody D24E4 whole-mount staining in WT 8dpf larvae. Staining labels the entire biliary system. (A') Staining of *taz-/-* larvae with this antibody results in the loss of this signal. *n=9* WT, *n=4 taz-/-*, (B') Staining of *yap-/-* larvae with this antibody is indistinguishable from WT siblings. *n=6* WT *n=3 yap-/-*.

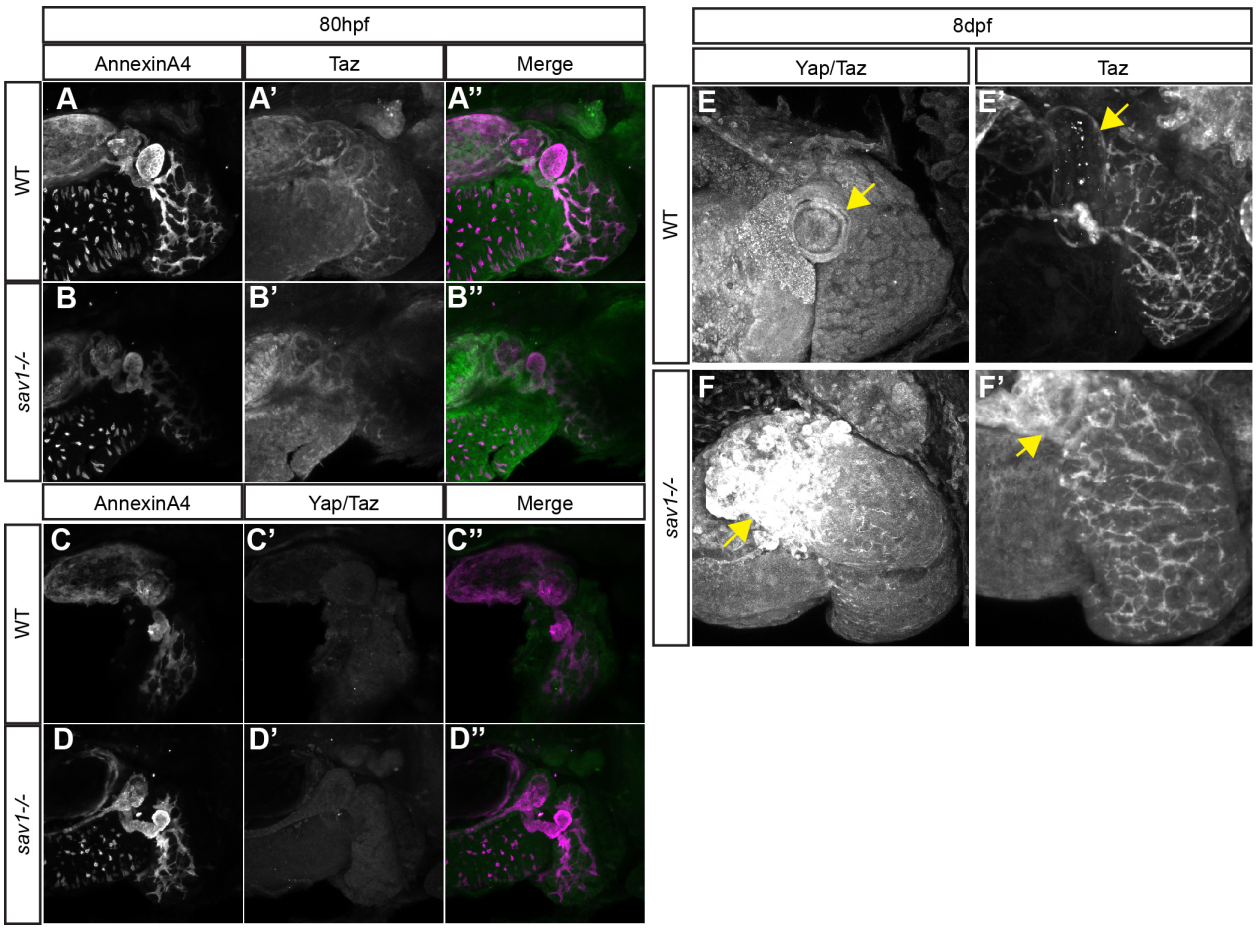

Figure S5. Comparison of Yap/Taz staining and Taz staining in WT and *sav1-/-* larvae. (A-B'') Taz and AnnexinA4 double staining at 80hpf reveal that Taz is enriched in the WT biliary system and unaltered in *sav1-/-* mutants, *n=3* WT; *n=3 sav1-/-.* (C-D'') In contrast Yap/Taz and AnnexinA4 double staining at 80hpf reveals low levels of staining in liver and pancreas without enrichment in the biliary system. Yap/Taz staining is similar between WT larvae and *sav1-/-* mutants, *n=4* WT; *n=5 sav1-/-* (E) Yap/Taz whole-mount staining at 8dpf of WT larvae shows consistent levels of staining throughout liver and gallbladder. *n=6* WT (E') In contrast, Taz whole-mount staining at 8dpf is restricted to the biliary system. *n=15* WT (F) Yap/Taz staining of *sav1-/-* larvae shows increase fluorescent intensity, particularly in the normal anatomic location of the gallbladder. *n=9 sav1-/-.* (F') Taz staining of *sav1-/-* larvae also shows similar increases in fluorescent intensity at this position while retaining expression throughout the biliary system. *n=13 sav1-/-.* Yellow arrows indicate gallbladders in WT fish (A-A'), and the normal position of the gallbladder in *sav1-/-* siblings (B-B').

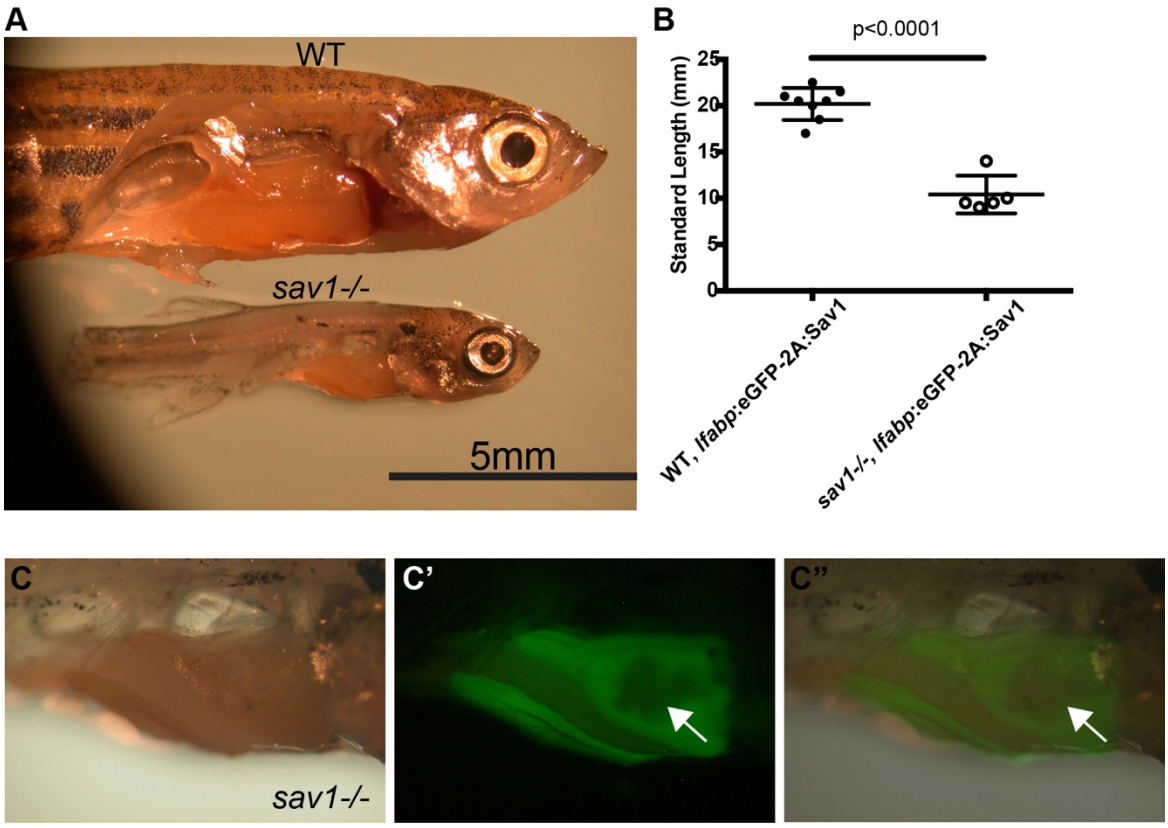

Figure S6. *sav1-/-*;*lfabp*:eGFP-2a:Sav1 fish are smaller than WT *lfabp*:eGFP-2a:Sav1 siblings and display regions of liver dysplasia. (A) Micrographs of WT and *sav1-/-* age-matched siblings transgenic for *lfabp*:eGFP-2a:Sav1 demonstrate the differences in size. (B) Quantification of (A). Standard length of zebrafish in millimeter (mm) shows that *sav1-/-;lfabp*:eGFP-2a:Sav1 fish are significantly smaller than their WT;*lfabp*:eGFP-2a:Sav1 siblings. *n=8* WT; *n=5 sav1-/-*. (C-C'') Brightfield and GFP fluorescent images of *sav1-/-;lfabp*:eGFP-2a:Sav1 liver, showing the loss of fluorescence present at the normal anatomical position of the gallbladder.

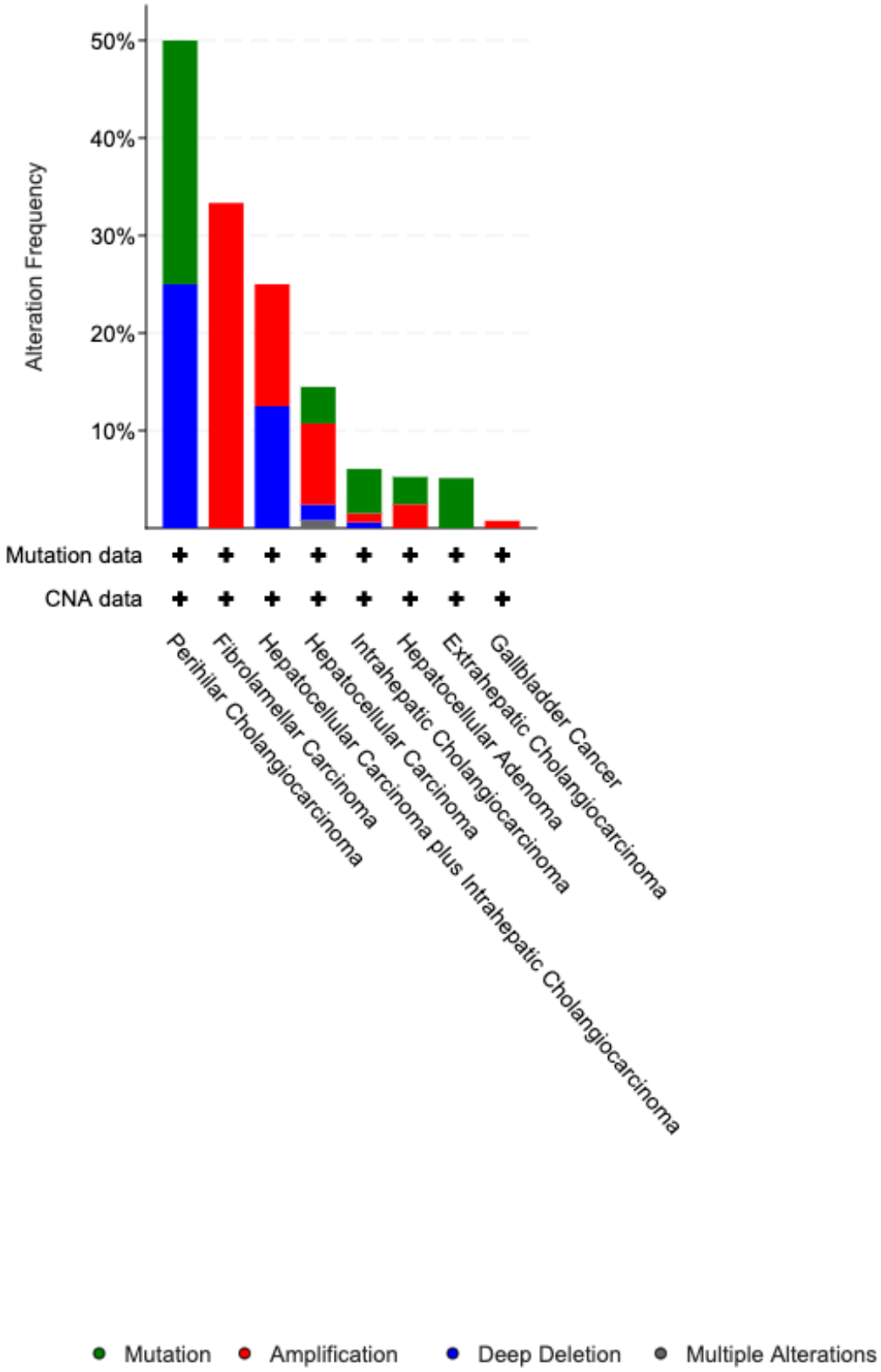

Figure S7. Genes for core Hippo pathway components are altered in biliary tract carcinomas. Data curated by cBioPortal from 15 studies on liver or biliary tract cancers were queried for alterations in the following core Hippo pathway components: SAV1, STK3, STK4, LATS1, LATS2, MOB1A, MOB1B, YAP1, and WWTR1. 151 of 1657 patient samples (~9%) had alterations in these Hippo pathway components. Furthermore, while the number of samples available for extrahepatic biliary tract cancers is relatively small compared to liver cancers generally, alterations in several Hippo pathway components are present. While only 4 samples of perihilar cholangiocarcinoma were available, 2 of these had alterations in the pathway, with 1 containing a deep deletion in SAV1, and the other a mutation in STK3. 39 cases were identified as extrahepatic cholangiocarcinoma, and 2 of these samples had mutations in YAP1. Finally, 1 out of 134 cases of gallbladder carcinomas were altered, identifying a LATS1 amplification. Y-axis represents the percentage of samples within the X-axis group that had alterations in at least one of the genes queried. CNA; copy number amplification.

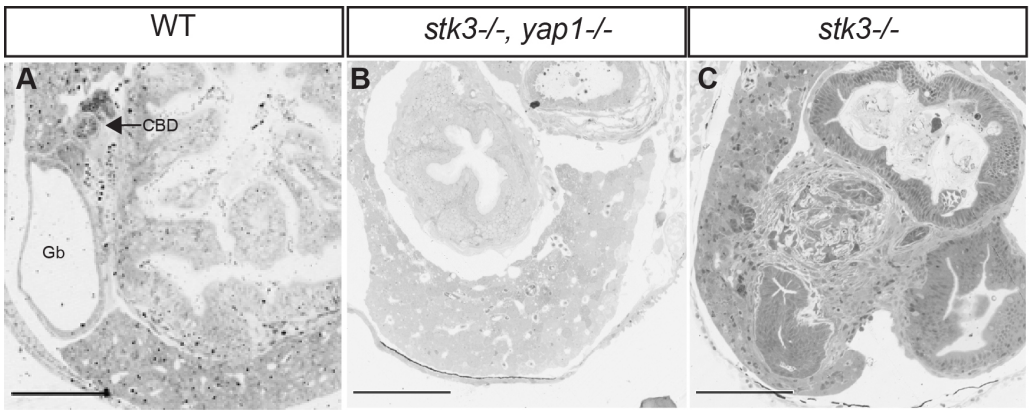

Figure S8. Loss of *yap* rescues abnormal biliary morphology in *stk3-/-* fish. (A-C) Toluidine Blue stained plastic sections of liver and gallbladder in WT, *stk3*-/-, and *stk3*-/-;*yap*-/- larvae at 16dpf, revealing rescue of gallbladder and common bile duct morphology. *n=5* WT; *n=3 stk3-/-*; *n=2 stk3-/-;yap-/-*. Gb; gallbladder, CBD; common bile duct.

	Perihilar Cholangiocarcinoma		Fibrolamellar Cholangiocarcinoma	Hepatocellular Carcinoma plus Intrahepatic Cholangiocarcinoma		Hepatocellular Carcinoma				Intrahepatic Cholangiocarcinoma			Hepatocellular Adenoma		Extrahepatic Cholangiocarcinoma	Gallbladder Carcinoma
	Mutation	Deep Deletion	Amplification	Amplification	Deep Deletion	Mutation	Amplification	Deep Deletion	Multiple Alterations	Mutation	Amplification	Deep Deletion	Mutation	Amplification	Mutation	Amplification
SAV1		1			1	1	2	3		3		2				
STK3	1		1	1		5	50	1	2		4		2	6		
STK4						2	1			1						
LATS1						13	1	8		2			2			1
LATS2						7	2	1		5			4	1		
MOB1A						1				1			1			
MOB1B							1									
YAP1						5	2	1		2					2	
WWTR1						3	10			1						
TOTAL ALTERATIONS	1	1	1	1	1	37	67	15	2	15	4	2	9	7	2	1
TOTAL CASES WITH ALTERATIONS	2		1	2		108				20			15		2	1
TOTAL CASES	4		3	8		746				330			286		39	134
ALTERATION FREQUENCY	50%		33.333%	25%		14.48%				6.606%			5.24%		5.13%	0.75%

Table S1. Genetic alterations to Hippo pathway components in biliary and liver carcinomas. Annotated summary of cBioPortal data of liver cancer subtypes associated with genetic alterations in Hippo pathway components.